Applied Geochemistry 194 (2025) 106590

Contents lists available at ScienceDirect

Applied Geochemistry

journal homepage: www.elsevier.com/locate/apgeochem

Mineral-driven persulfate activation: the role of recycled concrete alkalinity in oxidative water treatment

Chiara Cappelli [a,1,*], Albert Fernández-Lagunas [a], María Usieto [a], Mònica Rosell [a], Clara Torrentó [a,b], Cristina Domènech [a], Jordi Palau [a], Albert Soler [a]

[a] Grup MAiMA, SGR Mineralogia Aplicada, Geoquímica i Hidrogeologia (MAGH), Departament de Mineralogia, Petrologia i Geologia Aplicada, Facultat de Ciències de la Terra, Institut de Recerca de l'Aigua (IdRA), Universitat de Barcelona (UB), Martí Franquès s/n, 08028, Barcelona, Spain
[b] Serra Húnter Fellowship, Generalitat de Catalunya, Spain

ARTICLE INFO

Editorial handling by: G. Bird

Keywords:
Concrete dissolution
Hyperalkaline solution
Persulfate activation
In situ chemical oxidation (ISCO)
Circular economy

ABSTRACT

The dissolution of concrete—a prevalent anthropogenic material—generates hyperalkaline, Ca-rich leachates that may influence redox processes in subsurface environments. The knowledge of these geochemical processes serves as theoretical framework for the application of recycling concrete material to circular economy systems, providing sustainable alternatives to the concerning issue of the construction waste management while positively acting on specific environmental settings. This study investigates the potential of recycled concrete as a long-term alkaline activator for sodium persulfate in In Situ Chemical Oxidation groundwater treatments, with a focus on application in groundwater-recharge interception trenches in the vadose zone. A laboratory-scale study was conducted using flow-through columns filled with crushed recycled concrete, which was exposed to contaminated groundwater. The research assessed (i) the ability of concrete to generate and maintain alkaline conditions for persulfate activation, (ii) its mineralogical composition to determine reactivity and surface passivation, and (iii) chemical changes occurring upon persulfate addition at two different dosages. Results showed that recycled concrete effectively maintained high pH and buffered the system after persulfate injection, enabling efficient activation of the oxidant and substantial degradation of dissolved organic carbon. The system was controlled by the dissolution of concrete aggregates and cement phase together with the carbonation and (re)precipitation of new phases. The role of calcium and aluminium/magnesium silicate hydrates was proven to be crucial for the stability of the concrete microstructure and for maintaining the alkalinity. These findings demonstrate the dual role of recycled concrete for providing long-term alkaline activation of persulfate and mitigating clogging risks, supporting is practical use in groundwater remediation strategies promoting circular economy principles. Furthermore, these findings mirror processes observed in different hyperalkaline systems (e.g., radioactive waste repositories, CO_2 storage) where mineral-driven redox reactions control contaminant fate and/or carbon sequestration.

Terminology and definition index

Ordinary Portland Cement (OPC): most widely used type of cement, obtained by grinding clinker, gypsum, and other additives. The clinker itself is produced by sintering (at ~1400 °C) limestone, aluminosilicates (such as clay minerals), shale, and other secondary raw materials (iron ore, bauxite).

Blended Cement: produced by blending OPC with supplementary cementitious materials such as fly ash, slag cement, silica fume, or limestone.

Anhydrous phases of cement:

* Corresponding author.
E-mail address: chiaracappelli@ugr.es (C. Cappelli).
[1] Current institution: Department of Mineralogy and Petrology, Faculty of Sciences, University of Granada (UGR), Av. Fuentenueva s/n.

https://doi.org/10.1016/j.apgeochem.2025.106590
Received 2 May 2025; Received in revised form 25 September 2025; Accepted 11 October 2025
Available online 21 October 2025

Alite ($C_3\overline{S}$): Tricalciumsilicate ($3CaO\text{-}SiO_2$)
Belite ($C_2\overline{S}$): Dicalciumsilicate ($2CaO\text{-}SiO_2$)
Aluminate phase (C_3A): Tricalciumaluminate ($3CaO\text{-}Al_2O_3$);
Aluminoferrite phase (C_4AF): Tetracalciumaluminateferrite ($4CaO\text{-}Al_2O_3\text{-}Fe_2O_3$); Cement hydration products:

Calcium hydroxide (CH):

$Ca(OH)_2$, Portlandite, hydration product of $C_3\overline{S}$ and $C_2\overline{S}$.
Ettringite (AFt): $3CaO\text{-}Al_2O_3\text{-}3CaSO_4\text{-}32H_2O$, produced from sulfate-bearing cement phases (e.g., gypsum) and/or sulfate attack of the concrete.
Hydrated calcium aluminate (AFm): $Ca_2(Al,Fe)(OH)_6{\cdot}X{\cdot}xH_2O$ (X = singly or doubly charged anion)
Calcium Silicate Hydrate ($C\overline{S}H$) and calcium aluminum silicate hydrate ($CA\overline{S}H$): gel-like phase which aluminum and/or silicon, oxygen, and hydrogen atoms arrange in complex structures.

1. Introduction

Hyperalkaline environments form often after water interaction with anthropogenic material emplace in different settings (mining and waste sites, construction industries, radioactive repositories) (Gomes et al., 2016). In this context, the production and use of cementitious materials leave behind a considerable amount of alkaline residue. Concrete ranks as one of the extensively employed construction materials worldwide, finding applications in several infrastructures and buildings (De Brito and Saikia, 2012). Despite its high versatility, durability, and strength, the high demand of concrete raises concerns about the environmental impact primarily associated with the extraction and processing of raw materials, the energy-intensive manufacturing of cement (one of the main components of concrete), and the overall carbon footprint of the concrete industry (de Brito and Kurda, 2021). Consequently, there is a growing global initiative to generate and utilize construction materials that are more sustainable (Naik, 2008). Despite this effort, an enormous amount of concrete waste is constantly produced and is expected to increase in the future, contributing significantly to landfill space depletion and environmental stress. Therefore, there is an increasing attention to the recycling and cost-effective reuse of concrete (Kisku et al., 2017; Guo et al., 2018; Thomas et al., 2018; Verian et al., 2018; Wang et al., 2020). Beyond the reincorporation of the waste material to the construction chain, other circular economy strategies offer feasible and profitable alternatives (Ho et al., 2021).

In the present study, recycled concrete is tested as a novel material for the activation of sodium persulfate (PS), a strong oxidizing agent for the degradation of organic compounds in multi-contaminated groundwater. Traditional ex situ "pump and treat" treatment has been widely used for the elimination of organic pollutants from groundwater (Russell and Rabideau, A., 2000). More recently, in situ or hybrid in situ/ex situ systems have been employed to overcome the yield decreases of ex situ treatments and the potential issues arising from the extraction of large volumes of groundwater (i.e., high operating costs and energy consumption, large environmental footprint) (O'Connor et al., 2018; Xie et al., 2021; Ciampi et al., 2023). Among the in situ methods, In Situ Chemical Oxidation treatment (ISCO) has proven to be a highly efficient technology for the degradation of a wide variety of organic compounds (Krembs et al., 2010). ISCO involves the injection of a chemical oxidant into the contaminated area for the complete *mineralization* of the organic pollutants. Persulfate ($S_2O_8^{2-}$, PS) is one of the most used oxidants in ISCO treatments and its activation (i.e., initiation of radical generation) is a crucial step for the entire ISCO process due to the generation of radicals with higher redox potential than the PS anion itself (so called advanced oxidation). Among different possibilities, alkaline activation of persulfate may be summarized as follows (Furman et al., 2010):

$$S_2O_8^{2-} + 2H_2O \rightarrow 2SO_4^{2-} + HO_2^- + 3H^+ \text{ (base-catalyzed hydrolysis)} \quad \text{(Eq. 1)}$$

$$S_2O_8^{2-} + HO_2^- \rightarrow SO_4^{2-} + SO_4^{\bullet-} + O_2^{\bullet-} + H^+ \text{ (sulfate and superoxide radical anions generation)} \quad \text{(Eq. 2)}$$

$$SO_4^{\bullet-} + OH^- \rightarrow SO_4^{2-} + HO^{\bullet} \text{ (hydroxyl radical generation, only at alkaline pH)} \quad \text{(Eq. 3)}$$

This generation of hydroxyl radicals at alkaline pH causes a transition from $SO_4^{\bullet-}$-dominated to $HO^{\bullet}$-dominated oxidation process, which ultimately leads to the degradation of a wide range of organic compounds in solution. Such activation is usually achieved by the generation of alkaline conditions that are maintained by the periodic addition of large volumes of strong base solutions (e.g., NaOH or KOH). However, keeping the oxidant/activator at optimum levels is costly and requires constant monitoring. The alkalinity induced by concrete dissolution (dos Santos Macedo et al., 2019) may provide a low-cost solution for extending the operational period of ISCO treatments based on alkaline-activated persulfate. This alkaline-inducing capability of concrete has been previously used in approaches combining persulfate-based ISCO and in situ stabilization (ISS) for treating contaminated soils (Srivastava et al., 2016; Ma et al., 2018), but as far as we know has not been explored for water remediation. A previous field study at the Òdena contaminated site in Spain (Palau et al., 2014; Torrentó et al., 2014; Rodríguez-Fernández et al., 2018) demonstrated that groundwater-recharge interception trenches filled with recycled concrete, installed in the vadose zone, can effectively prevent only certain contaminants from reaching the aquifer (Torrentó et al., 2014). This effect is attributed to degradation by alkaline hydrolysis, promoted by the alkaline conditions generated by the recycled concrete. Additionally, this approach contributes to the reuse of a waste material. This system, thus, offers an ideal opportunity to investigate the use of recycled concrete as a long-term activator for PS in water remediation. Before field implementation, in the present study, a scaled down laboratory set-up was used to assess: (i) the capacity of recycled concrete in maintaining alkaline conditions, which is essential for the activation of PS and subsequent oxidation of contaminants through this treatment; (ii) the mineralogical characterization of the concrete, in order to evaluate mineral reactivity and possible passivation of reactive surfaces, and (iii) chemical changes in solution upon persulfate application at two different dosage levels. Flow-through columns were filled with grinded concrete waste and exposed to two different types of water: alkaline water collected from the interception trenches and neutral-pH aquifer water, both extracted from the Òdena site. Later, a punctual PS injection was performed, and the system was monitored over the experimental time. The results set the basis for future in situ implementation of a similar remediation approach, as already planned for the Òdena site after the present lab-based experimentation. Furthermore, secondary emerging knowledge may be useful in different contexts, such as carbon sequestration and radioactive waste repositories, where concrete reactivity and durability define the successfulness of the strategy.

2. Material and methods

2.1. Materials

Recycled concrete gravel (RCG) in the size range 8–12 mm was supplied by the company H-ZERO (Terrassa, Barcelona, Spain). The material fell into the category of recycled aggregates with the following limits: >95 wt% of non-bound and/or hydraulically bound aggregates, concrete, and concrete products, <10 wt% of ceramic elements and other materials associated with masonry pieces, and a small fraction (<1 wt%) of other materials (bituminous and floating among others) (European standard EN 933-11). To obtain representative samples, the concrete gravel was split using a mechanical splitter into four batches (~3.6 kg each). The solid was then sieved and rinsed for a few seconds with deionized water to remove fine particulate and left to dry for 24 h at room temperature before being used.

The RCG was exposed in flow-through systems to two different solutions collected from the Òdena contaminated site: 1. aquifer water (AW, pH ~ 7), collected from S8 piezometer, and used in the Blank column to simulate newly recharge water entering the interception trench for the first time; and 2. alkaline water from one of the interception trenches (TW, pH ~ 11), already equilibrated with concrete gravels placed in the trench since 2006 (Palau et al., 2014; Torrentó et al., 2014; Rodríguez-Fernández et al., 2018). The AW water served as control for assuring the effective alkalinization effect of the gravel; the TW solution was the contaminated water collected from the field system where future implementation of the ISCO treatment is foreseen. Approximately 10 L of AW and 40 L of TW were collected across three field campaigns conducted during the first five months of 2023. Sodium persulfate ($Na_2S_2O_8$) was purchased from Sigma-Aldrich (reagent grade, ≥98 %) and used to prepare two solutions with a different concentration (7 g L^{-1} and 70 g L^{-1}) in 2 L of TW each to inject into the columns.

2.2. Experimental set-up

Four cylindrical columns made of polymethyl methacrylate (PMMA) were constructed as flow cells, mimicking field groundwater-recharge interception trenches, for the gravel reaction experiments (Fig. 1). Each column consisted of a lower chamber (5 cm high and 11.4 cm internal diameter) to accumulate the inlet solution, and an upper reaction chamber (25 cm high, same diameter) filled with approximately 3.6 kg of gravel. The chambers were separated by a perforated platform (hole diameter ~4 mm), which was covered with polytetrafluoroethylene (PTFE) boiling stones of approximately 6 mm in diameter. To prevent the generation of preferential flow paths and to promote good homogenization of the inlet solution, a magnetic stirrer was placed in the lower chamber to agitate the inlet solution during the injection of the oxidant.

A peristaltic pump (ISMATEC™) was used to inject the inlet solution into the column through Pharmed tubes (TPE). Tubes of PTFE with different diameters were used to connect the elements of the flow system (inlet bottle, pump, column, and outlet solution bottles). The solution was injected in the column through a PMMA fissured tube (~4 mm diameter) directly immersed in the lower chamber (Fig. 1).

The columns were fully filled with the AW or TW solutions over ~12 h, after which the solid was allowed to condition for 1 week at room temperature. An average column porosity of 58 ± 1 % was estimated by calculating the difference between the weight of the columns with gravel in contact with the solution (for a contact time >48 h) and the weight of the columns with only gravel.

After the conditioning time, the flow-through experiments were started at controlled room temperature (25 ± 2 °C) and a flow rate of ~0.03 mL min^{-1}. This flow rate is representative of the solution residence time in the interception trench in the vadose zone of Òdena field site, calculated by Torrentó et al. (2014). Initially, persulfate-free solutions were used. After ~900 h, the injection of sodium PS was performed in two of the columns. Throughout the experiments, both the inlet and outlet solutions were stored in polypropylene (PP) bottles. Outlet solutions were sampled every 48–72 h, whereas inlet samples were taken at 0 and 500 h of the experimental time and any time the inlet solution was changed to freshly field collected water.

Four different experimental setups were used (Table 1):

Table 1
Input solution and flow rates of each experiment. Note that the solution injection at rapid flow rate was performed at ~900 h reaction time (except for Blank experiment). AW = aquifer water; TW = interception trench water.

Experiment	Solution	Flow rate before and after injection	Flow rate during the 12 h injection
Blank	AW	0.03 mL min^{-1}	–
Ctrl	TW	0.03 mL min^{-1}	2.78 mL min^{-1} TW persulfate-free solution
PSmin	TW	0.03 mL min^{-1}	2.78 mL min^{-1} TW + persulfate 7 g L^{-1}
PSmax	TW	0.03 mL min^{-1}	2.78 mL min^{-1} TW + persulfate 70 g L^{-1}

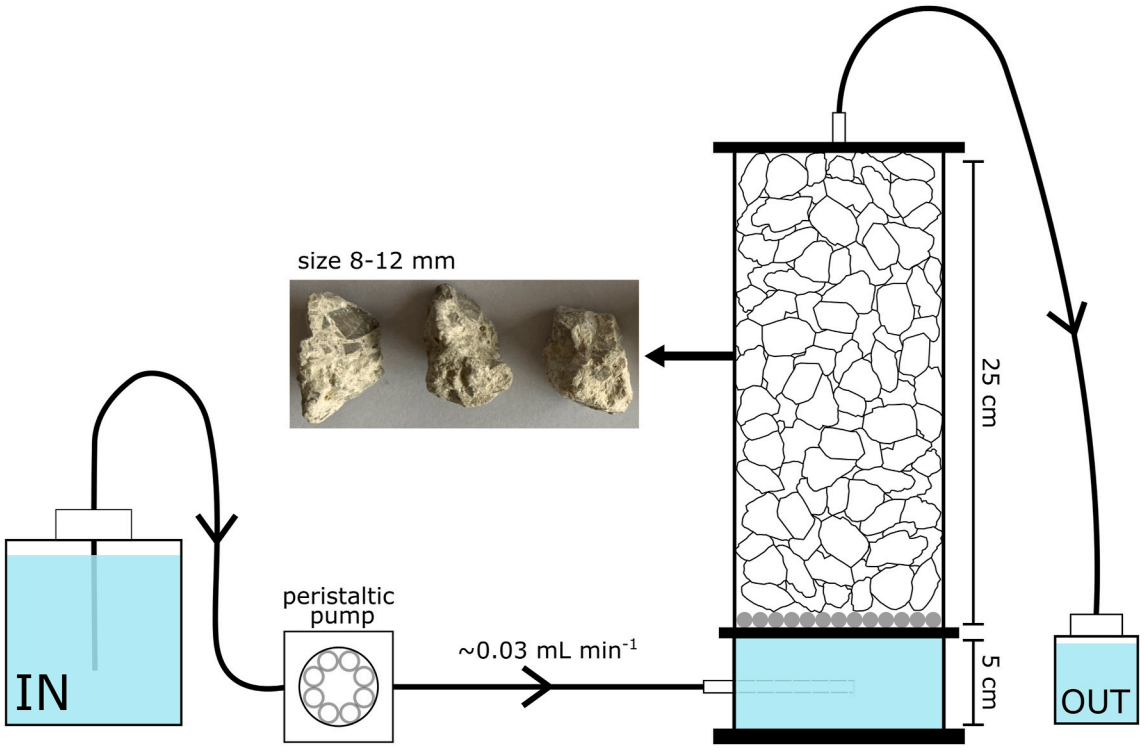

Fig. 1. Schematic diagram of the mounted flow-through system for the simulation of a circulating solution through recycled concrete gravel, such as the field groundwater-recharge interception trench in Òdena. Four parallel systems were used in this study.

i. Blank: gravel reacting with the AW. It simulates a brand-new constructed groundwater-recharge interception system, or other potential groundwater remediation applications.
ii. Control (Ctrl): gravel reacting with the TW (without oxidant injection). It serves as PS-free reference for the correct evaluation of the oxidation treatment.
iii. & iv. Persulfate minimum (PSmin) and maximum (PSmax): gravel reacting with the PS-enriched TW (at 7 and 70 g L^{-1}, respectively), after a first reaction time with only TW solution (PS-free solution, up to ~900 h).

In PSmin and PSmax experiments, the enriched-persulfate solution was injected over 12 h at a rapid flow (2.78 mL min^{-1}) simulating an injection event in the field. The inlet solution was then replaced with fresh TW and the flow was restabilized to ~0.03 mL min^{-1}. The control column (Ctrl) was treated similarly to monitor the effect of the flow change and to compare the solid behaviour during reaction with and without oxidant. In the Blank experiment, however, flow rate was maintained at 0.03 mL min^{-1} throughout all the experimental duration (Table 1).

At the end of the experiments, the solid was retrieved from each column and treated with isopropanol to accelerate the evaporation of water from the concrete fragments to avoid post-experimental carbonation (Snellings et al., 2018; Zhang and Scherer, 2021). The isopropanol was then allowed to evaporate, at room temperature in a N_2 saturated chamber, and the dried solid was stored in desiccator boxes.

2.3. Analytical methods

The RCG was characterized before and after the conditioning time and once the reaction experiments were ended by: optical microscopy (Nikon Eclipse LV 100POL); X-ray diffraction (PANalytical X'Pert PRO MPD) hosted at the Scientific and Technological Centers of the University of Barcelona (CCiT-UB) and operating in reflection mode using Cu $K\alpha_1$ emission (from 4 to 100° with 0.026° step size and 96.39 s measuring time); scanning electron microscopy (SEM, Quanta 200 equipped with backscattering (BS) and energy dispersive detector (EDS)) hosted at the CCiT-UB; and thermogravimetry (Shimadzu TGA-50H analyzer equipped with a Mettler-Toledo AX26 Delta Range microbalance) hosted at the University of Granada (UGR). The chemical composition of the starting and the reacted RCG was also determined by X-ray fluorescence spectrometry (XRF, PANalytical model Zetium, equipped with a Rodium X-ray tube) at the Scientific Instrumentation Center of the UGR. Free and forced water absorption assays (Institution, 2008) were performed on a representative amount (~60 g) of each sample to evaluate possible porosity variation after the solid reaction.

Chemical water composition, pH and electrical conductivity (EC) were determined during the experiments for both inlet and outlet solutions. The pH and EC were measured by an electrode SenTix® 940 and a sensor TetraCon™ 925, respectively. The instrumental precision was estimated to be ±0.1 for the pH and 1 % for the EC.

The solutions were characterized at CCiT-UB for:

- Dissolved organic and inorganic carbon (DOC and DIC, respectively) by ANALYTIK JENA multi N/C 3100 whose detection limit is 0.5 mg L^{-1} and analytical error 2 %. Note that the DOC measurement was taken as representative of the organic matter (OM) in solution.
- Cation's (Mg, Ca, Na, K, Si, Al, Fe) concentration by Inductively Coupled Plasma Optical Emission and Mass Spectrometry (ICP-OES, ICP-MS). The ICP-OES detection limits for Mg, Ca, Na, K, Si and Al are 0.10, 2, 5, 1, 0.5 and 0.2 mg L^{-1}, respectively, and the analytical error is 2 %. The ICP-MS detection limits for Al and Mg, and Fe are 2 and 6 μg L^{-1}, respectively, and the analytical error is 3 %.
- Anion's (sulfate and chloride) concentration by liquid chromatography using a Jasco equipment with a Dionex BioLC ED50 electrochemical detector. The detection limit is < 0.4 mg L^{-1} and the analytical error is 1 %.

For each sample and analysis, a liquid aliquot was filtered by a FilterBio®, PTFE-L 0.45 or 0.22 μm (the latter for ICP-OES and ICP-MS analyses) and stored in the dark at 4 °C before measurement. The aliquots for cations determination were acidified with nitric acid (HNO_3 69 %, reagent grade) before storage.

The chemical composition of the inlet and outlet solutions was used for calculating the solution saturation index (SI) for concrete mineral phases and possibly new phases to support the microscopy observations of the initial and reacted RCG. The SI of a solution with respect to a mineral phase is expressed as SI = log(IAP/K), where IAP is the ion activity product of those ions involved in the dissolution of the mineral and K is its solubility constant (equilibrium constant for the dissolution of the mineral). Moving from equilibrium conditions (SI = 0), the solution can become oversaturated (SI > 0) or undersaturated (SI < 0) with respect to a specific mineral phase. In an oversaturated state, the mineral may precipitate, while in an undersaturated state, the mineral may dissolve if it is already present in the system. SI calculations for selected solid phases were performed using the code PHREEQC v3 (Parkhurst et al., 2013) and the thermodynamic database ThermoChimie v12a (Giffaut et al., 2014), which was modified by introducing persulfate. Temperature was set constant at 25 °C.

3. Results

3.1. Solution analysis

The pH of the outlet solutions increased over the first ~280 and 400 h after the conditioned solid was immersed in the AW (pH ~7) and TW (pH ~11) solutions, reaching average values of ~11.8 and 12.1, respectively (Fig. 2, AW-Blank column, TW-Ctrl/PS columns). This confirms the strong alkalinization and buffering effect of the RCG across the studied pH range. The experiment with AW (Blank) demonstrated that freshly recycled concrete possesses a high buffering capacity, effectively raising the pH of neutral groundwater, such as that recharging the Òdena aquifer. The results of the experiments with TW highlighted the sustained buffering capacity of concrete gravel that has been conditioned in the field over the long term. After the temporary change of the flow rate (Ctrl and PS columns) and the persulfate injection (only in the PS columns) at ~900 h, the pH dropped to values of 11.9, 11.7 and 9.8, in the Ctrl, PSmin and PSmax experiments, respectively. The pH slowly recovered higher values, reaching again a value of ~12 before the end of the Ctrl (at ~2280 h) and PSmin (at ~2690 h) experiments, whereas staying to a slightly lower value of ~11.7 for the PSmax experiment.

In the columns with TW solution, the EC underwent a slight decrease with respect to the initial value of ~2.5 mS cm^{-1} during the first ~150 h of the experiments to increase then rapidly to an average value of ~2.7 mS cm^{-1} (Fig. 2). As a consequence of the PS injection, the EC greatly increased to 7.8 and 44.4 mS cm^{-1} for the PSmin and PSmax experiments while it stabilized at values similar to the inlet solution in the Ctrl column after the flow rate variation. Starting at ~1200 h experiment time and with the fresh TW solution circulating in the systems, a gradual decrease in EC was observed in the PSmin and PSmax columns, reaching values of 3.7 and 13.2 by the end of the experiments, respectively. In the column with AW-solution (Blank), the EC maintained an average value close to the inlet solution of ~2.6 mS cm^{-1}.

Comparing the inlet and the outlet solutions during the stabilization time (~900 h) before persulfate injection, a decrease of Ca and Mg and an increase of Na and K was observed in all experiments (Fig. 3). Notably, the Mg concentration in the AW inlet solution was three orders of magnitude higher than in the outlet solution, revealing the precipitation of secondary phases or/and the uptake of Mg into labile phases such as sorbed complexes. The injection of PS lead to a sharp increase in

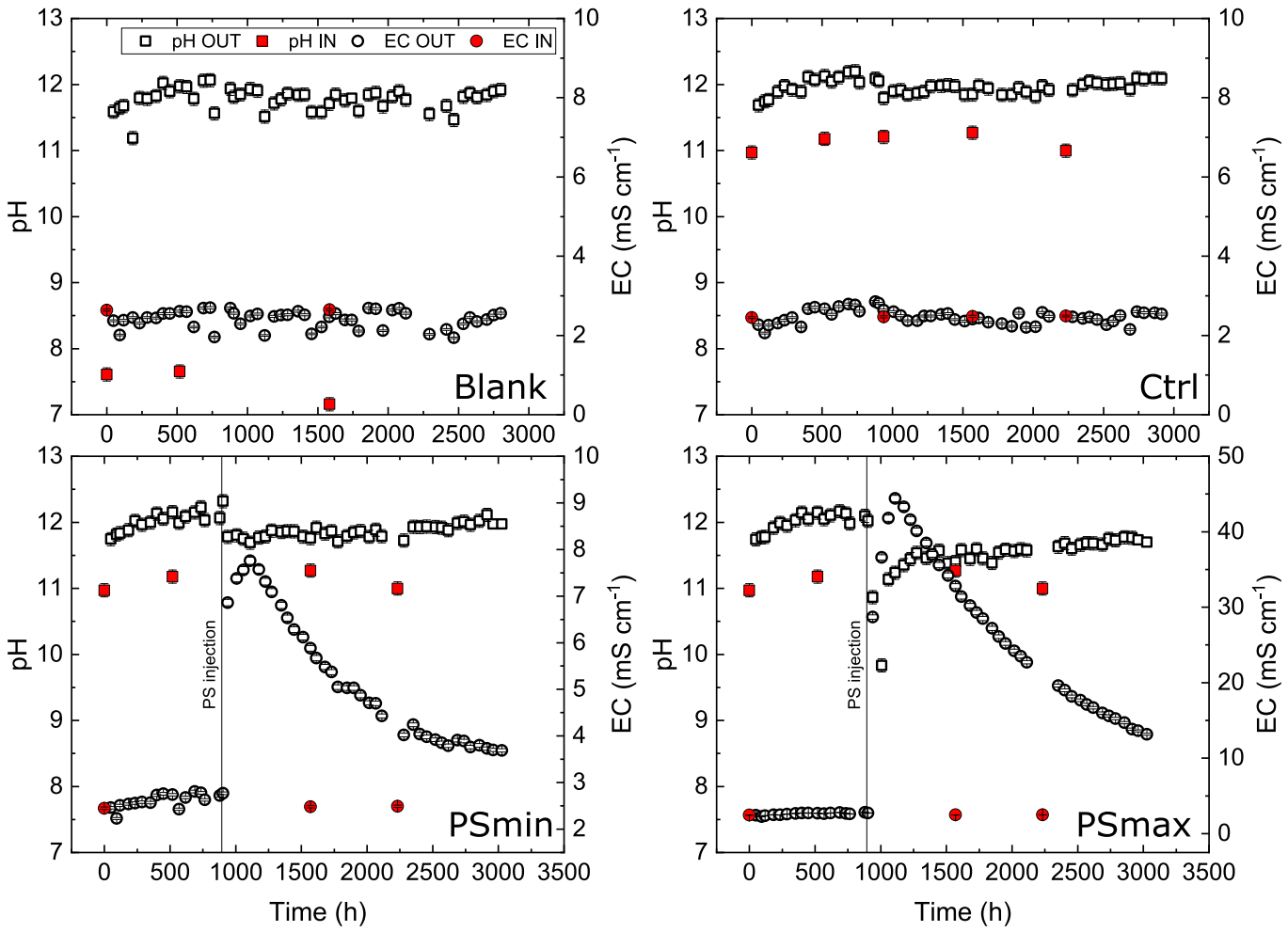

Fig. 2. Electric conductivity (EC) and pH of the inlet and outlet solution for each flow-through experiment, measured periodically over the experimental time lapse. Error bars display the analytical uncertainty, and, in some cases, they are smaller than the symbols.

Ca, Mg, Na and K concentrations in the outlet solutions, especially for the PSmax experiment, followed by a gradual decline. Note that the flow of the Ctrl experiment was also transiently increased (simulating the injection event) to maintain a good reference for the ISCO treatment. In the Ctrl experiment, while the Ca and Mg exhibited a similar trend than in the PS experiments (Fig. 3a and b), the flow increase resulted in an initial K and Na concentration decrease (Fig. 3c and d).

The Si and Al concentrations in the outlet solutions were higher than in the inlet solutions (Fig. 4a and b). The leaching of Si was immediate, with concentrations at the beginning of the experiment 6–7 times higher than in the inlet solution, being more evident in the Blank column, followed by a decreasing tendency with time. Al concentration in the outlet solutions, however, increased progressively with time from the initial concentration of the inlet solutions, before the injection of persulfate, being slightly higher in the Ctrl experiment. The temporary flow rate increase (and PS injection) resulted in a sharp drop in Si concentration that recovered quite rapidly up to a steady state at the experimental time of ~2000–2200 h. In this moment, for the Ctrl experiment, the concentration reached values near to those of the input solution. Similar to Si, the Al concentration underwent a drop with the change of the flow rate, however, when the rate was reset to the initial value, Al concentration clearly increased only for the Ctrl experiment. Note that the Al concentration of both inlet solutions (AW, TW) slightly decreased with time after the first ~900 h due probably to aluminum hydroxide precipitation. For Fe, concentrations at the beginning of the experiment (<900 h) were also higher in the outlet solutions than in the inlet solutions (Fig. 4c). Fe concentrations showed a trend similar to Si, reaching a steady state at values near to the those of the inlet solution for all the experiments, except for the PSmax experiment, where data dispersion was observed.

Regarding the anions, the SO_4^{2-} concentration (Fig. 5a) decreased as the solution passed through the columns, hinting to the formation of S-phases comparing outlet and inlet solutions in the pre-injection period. Once PS was injected, and according to the formation of sulfate during the activation of the oxidant (Eq. (1)-3), a significant increase in the sulfate content was observed in both the PSmin and PSmax columns with respect to the Ctrl experiment. In contrast, the temporary increase of the flow rate in the Ctrl experiment induced the sulfate concentration to rise to values close to TW-inlet and rapidly decrease to the observed pre-injection outlet values. Compared to the sulfate concentration in the TW-inlet solution (10 mM), sulfate values remained close to this concentration in the PSmin column, whereas values were up to 3.5 times larger in the PSmax column. The Cl^- concentration (Fig. 5b) tended to remain stable over time, with values in the outlet solutions close to and slightly higher than the inlet values for the AW experiment (Blank) and the TW experiments (Ctrl, PSmin and PSmax), respectively. Again, the effect of the flow rate change is visible.

Overall, the DIC (Fig. 6a) in the outlet solution remained stable and close to the inlet values during the TW-solution experiments. To the contrary, the DIC of the outlet solution of the AW experiment (Blank) was much lower than in the inlet solution, showing an increase after ~500 h, finally recovering values close to the other experiments (<10 mgC L^{-1}).

The initial DOC values measured at the outlet solution for each

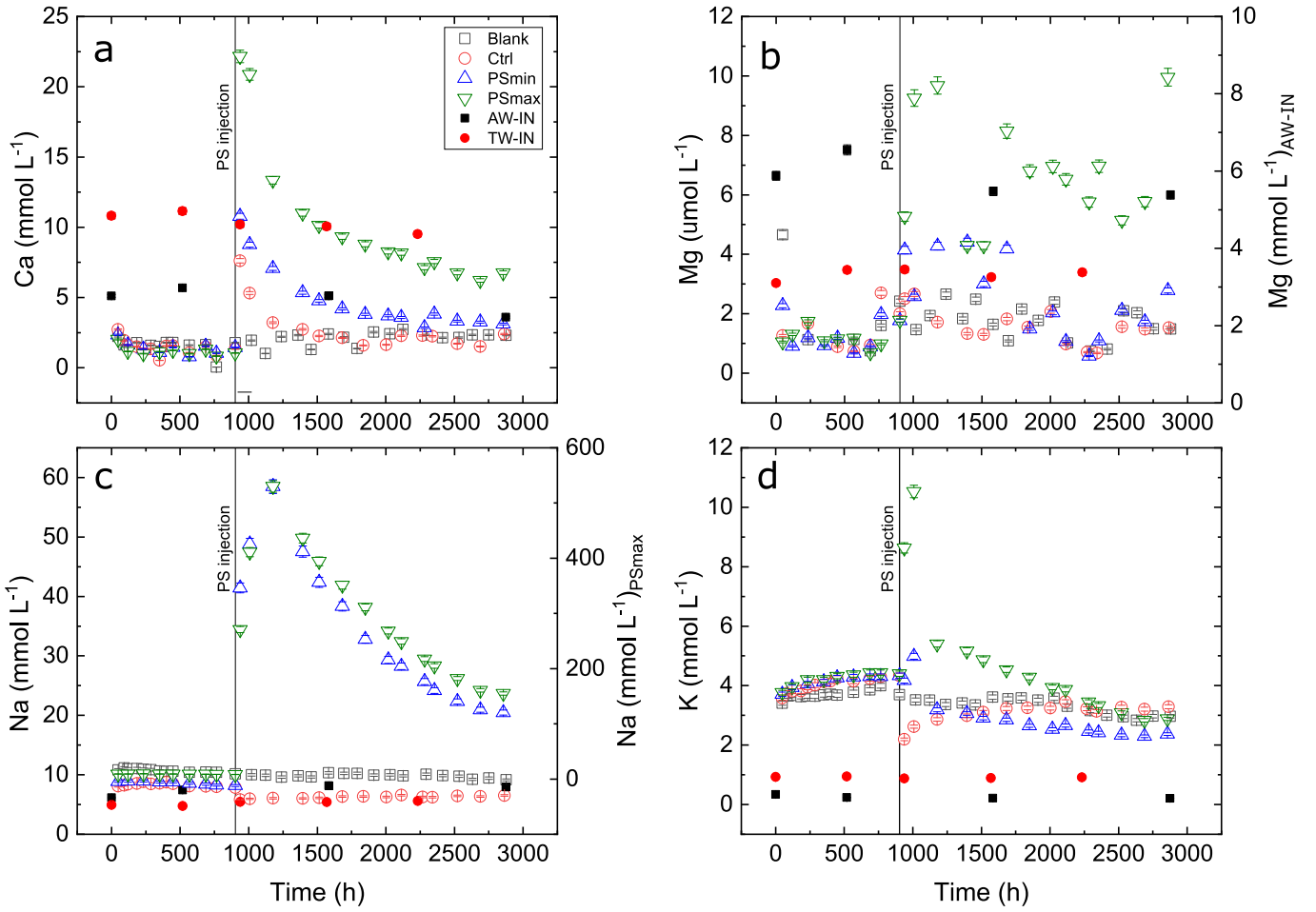

Fig. 3. Total Ca (a), Mg (b), Na (c) and K (d) concentration of the inlet and outlet solution of each of the flow-through experiments, measured periodically over the experimental time lapse. The vertical line in each plot indicates the time of the PS injection (for PSmin and PSmax) and the temporary flow rate increase into the columns (except for the Blank). Note that a secondary y-axis is used in plots (b) and (c) to accommodate the higher Mg and Na contents the inlet solution of the Blank experiment (AW-IN) and in the outlet solution of the PSmax experiment, respectively. Error bars display the analytical uncertainty and, in some cases, they are smaller than the symbols.

experiment were higher than those in the inlet solution (Fig. 6b), followed by a similar decreasing tendency for all the experiments previous to the oxidant injection. The persulfate injection and/or the flow rate increase provoked a sharper decrease in the DOC of the TW experiments that fell below the inlet value in the PSmax column (ranging between 0.5 and 2 mgC L^{-1}), while it reached values close to the inlet solution in the other columns.

3.2. Solution saturation indexes

The SI of the most relevant mineral phases were calculated for the different outlet solutions (blank, Ctrl, PSmin and PSmax) and the AW and TW inlet waters (Table S1 in Supplementary Material). Several mineral phases were found close to the equilibrium (SI = 0) or at a supersaturation state (SI > 0), suggesting their precipitation during the experiments (e.g., CSH phases, AFt, calcite, hydrotalcite, ferrihydrite and goethite). Aluminium phases saturation index varied through the experiment timelapse. Notable, the SI of brucite presents slightly positive or close to equilibrium values, reaching its highest values at the end of the experiment (t = 2860 h) in PSmax ($SI_{Brucite}$ = 1.0) and PSmin ($SI_{Brucite}$ = 0.7) columns. The SI of ettringite becomes more positive towards the end in the blank experiment ($SI_{Ettringite}$ = 1.5) while in the Ctrl, PSmax and PSmin experiments, $SI_{Ettringite}$ increases abruptly from ~ −1.0 to ~ 4.0 after the injection of persulfate or fresh TW (t ~ 900 h) and then, decreases progressively to slightly negative values ($SI_{Ettringite}$ = −0.4) in the Ctrl column or less positive values ($SI_{Ettringite}$ ~ 3.0) in the PSmax and PSmin columns. Mineral phases presenting an undersaturated state (SI < 0) include CASH and AFm phases, dolomite, portlandite, gibbsite, gypsum and quartz.

3.3. Optical microscopy

The RCG used in the flow-through system comprised aggregates and cement (OPC and blended cement), exhibiting variations ranging from single lithology compositions to monomictic and polymictic microconglomerates (see Fig. S1 in Supplementary Material). Belite ($C_2\overline{S}$) and alite ($C_3\overline{S}$) were identified among the minor minerals within the cement paste of several grains, whereas clumps of acicular minerals, likely ettringite, occupied voids and grain edges (Fig. 7a–c). The belite was surrounded by a brown-colored phase, most probably aluminoferrite, while the dark layers between crystals are likely C $\overline{S}$ H hydration products, which were also present as amorphous phase distributed among ettringite acicular crystals (Fig. 7b and c).

The grains retrieved at the end of the reaction experiments manifested in all cases a conspicuous alteration and the presence of cement hydration products. In particular, massive acicular crystals filled voids and coated the surface of the concrete, especially after persulfate solution was circulated through the columns PSmin and PSmax. In addition, gel-like material often occupied the solid porosities (Fig. 7d–e). As SEM-EDS results suggest (see section 3.7 and "SEM/EDS" in Supplementary

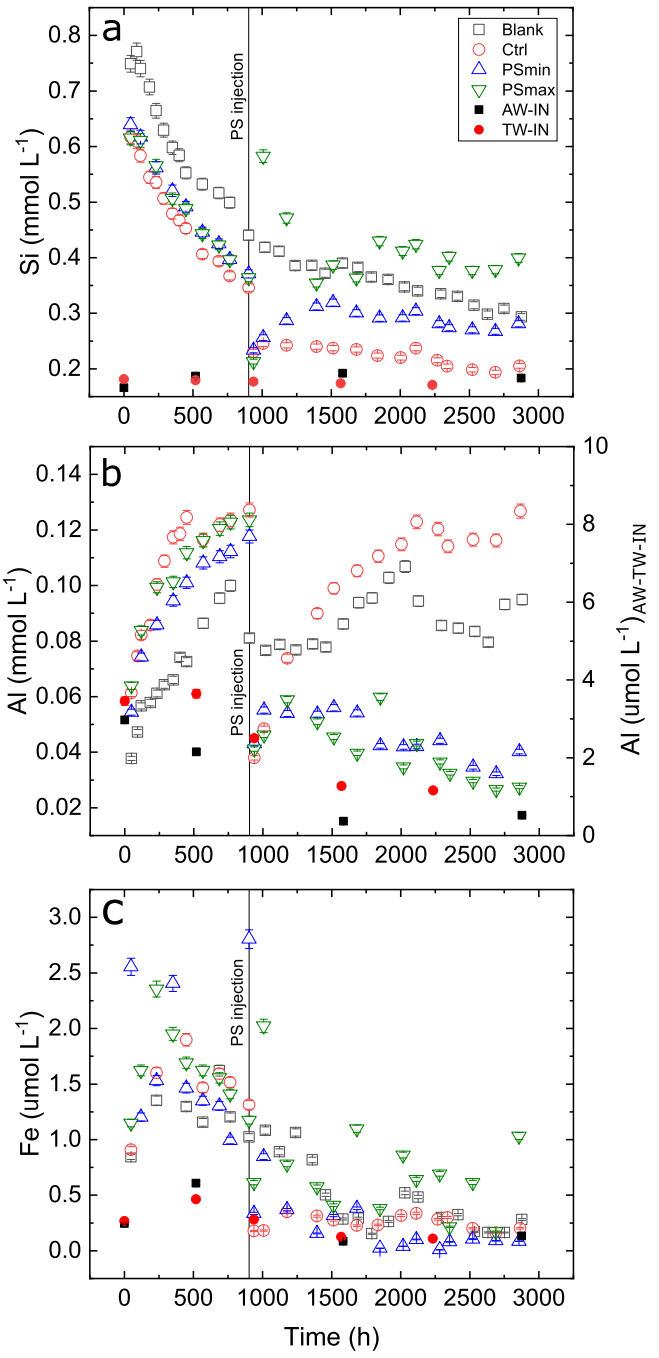

Fig. 4. Total Si (a), Al (b) and Fe (c) concentration of the inlet and outlet solution of each of the flow-through experiments, measured periodically over the experimental time lapse. The lines in each graph indicate the time of the PS injection (for PSmin and PSmax) and the temporary flow rate increase into the columns (except for Blank). Error bars display the analytical uncertainty, and, in some cases, they are smaller than the symbols.

Material) small amount of thaumasite probably formed, epitaxially growing on the acicular crystals of ettringite. Calcite crystals precipitated into fractures and porosities, forming veins and coating voids edges of all the grains (Fig. 7 f).

3.4. X-ray fluorescence

The chemical composition of the starting material and the four differently treated RCG samples after experimental time (Table 2) presented minimal variation overall, but some significant differences were observed. The Blank and the Control samples exhibited lower contents of SiO_2, Al_2O_3 and Fe_2O_3, and higher and slightly higher contents of CaO and MgO, respectively, than the initial solid (RCG-IN). Conversely, the PS-treated samples displayed the opposite trend. Furthermore, the Na_2O content increased in the samples reacted with the TW solution, and SO_3 raised in all the treated samples, being higher in the solids treated with persulfate solutions. Additionally, in those samples reacted with persulfate, the loss on ignition (LOI) decreased notably.

3.5. X-ray diffraction

The mineral phases of the concrete aggregates (i.e., sand, gravel) are almost invariant despite the gravel interaction with the different solutions and are clearly visible in the solid diffractograms (Fig. 8), with intense peaks corresponding to calcite, dolomite, quartz, feldspars and phyllosilicates, reflecting the lithological diversity of the material (see section 3.3 the "Optical microscopy" section). To the contrary, the cementitious phases, especially the almost absent anhydrous ones, do not show clear peaks, often masked/overlapped by the aggregate peaks. Nevertheless, tobermorite-14A and oyelite as end members for the low Ca/Si ratio, and jaffeite for the high Ca/Si ratio were identified as C $\overline{S}$ H phases. In addition, the contribution of portlandite to the 4,91 Å peak (2Theta 18,0) must be taken in account. Ettringite was certainly present as hydrous calcium-aluminum sulfate cement product, being more abundant in the PSmax treated sample. In this sample, a high peak at 1.99 Å (2Theta 45,4) appeared, likely associated with the argillitic phase of the altered solid. It is worth noting that the intensity of the dolomite peaks decreased after solid alteration.

3.6. Thermogravimetry analysis

Thermogravimetry (TG) and Differential Thermogravimetry (DTG) plots were obtained for the initial and reacted RCG samples. TG measures the change in mass (or weight loss %) of a sample as a function of temperature, while DTG measures the rate of mass change. The presence of typical concrete phases was graphed (Figs. 9 and 10). In particular, relative total weight losses in the temperature ranges of 25–120 °C and 550–900 °C are indicative of ettringite and calcite decomposition, respectively (Fig. 9) (Villain et al., 2007; Wang et al., 2024). Interestingly, in the sample retrieved after the PSmax experiment a shift of the peaks towards higher temperatures was observed, and a new small peak overlapping the ettringite peak appeared, pointing to the formation of gypsum and/or AFm phases (Fig. 10b) (Wang et al., 2024). In addition, a bulge of the big $CaCO_3$ peak in the DTG curves was identified, being almost absent for the starting material (IN sample) but became more evident in the sample retrieved after the Ctrl experiment (red curve in Fig. 10b) and it likely corresponded to dissociation of calcite formed after carbonation (Deloye and Divet, 1992; Villain et al., 2007). Notably, the peak around 450 °C typical of portlandite dihydroxylation (Villain et al., 2007) is absent in all the plots, indicating that this phase has been almost totally dissolved during the lifespan of the starting material and did not form in significant amount after the hydration of the cement anhydrous phases during the solid/water reaction.

The relative weight loss for each phase and sample was calculated from the TG diagrams taking in account the temperature ranges of the peaks identified in the DTG diagrams (Table 3). It was assumed that in the temperature range between ~200 and 600 °C organic matter decomposes, and that C $\overline{S}$ H may also decompose before the more stable calcite.

3.7. Scanning electron microscopy

The SEM-EDS analysis of the starting and conditioned RCG (after one week of soaking in TW, see section 2 "Materials and Methods"), revealed the presence of anhydrous phases of the cement [i.e., alite ($C_3\overline{S}$), belite

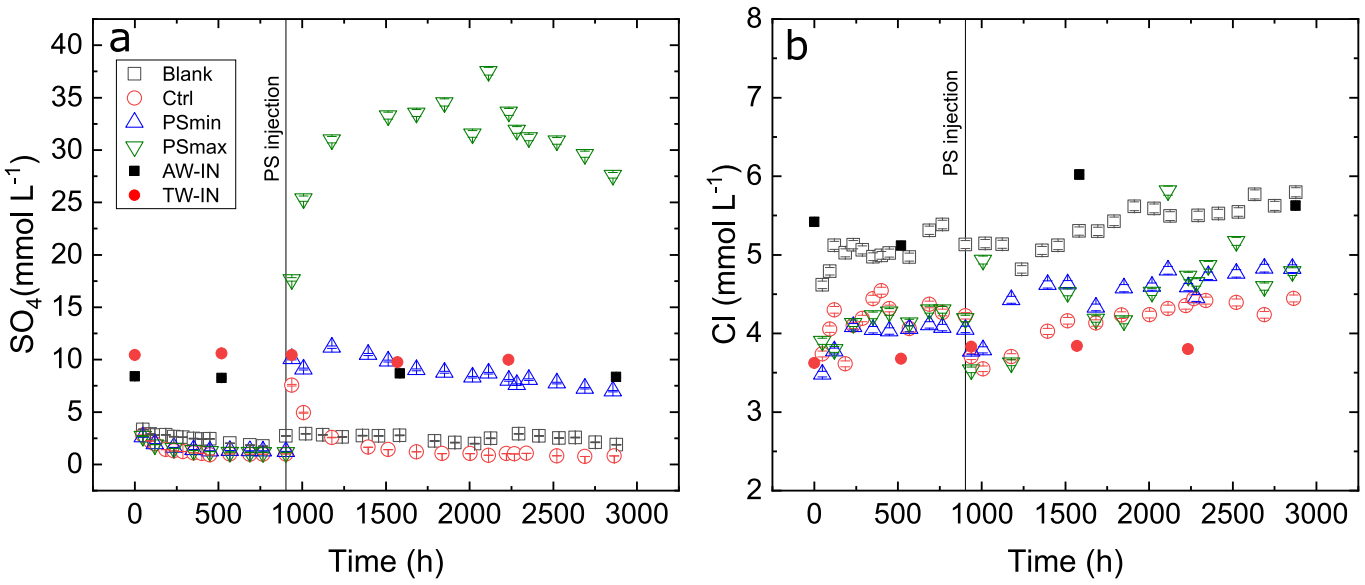

Fig. 5. Sulfate (a) and chloride (b) concentration of the inlet and outlet solution of each of the flow-through experiments, measured periodically over the experimental time lapse. The lines in each graph indicate the time of the PS injection (for PSmin and PSmax) and the temporary flow rate increase into the columns (except for Blank). Error bars display the analytical uncertainty and, in some cases, they are smaller than the symbols.

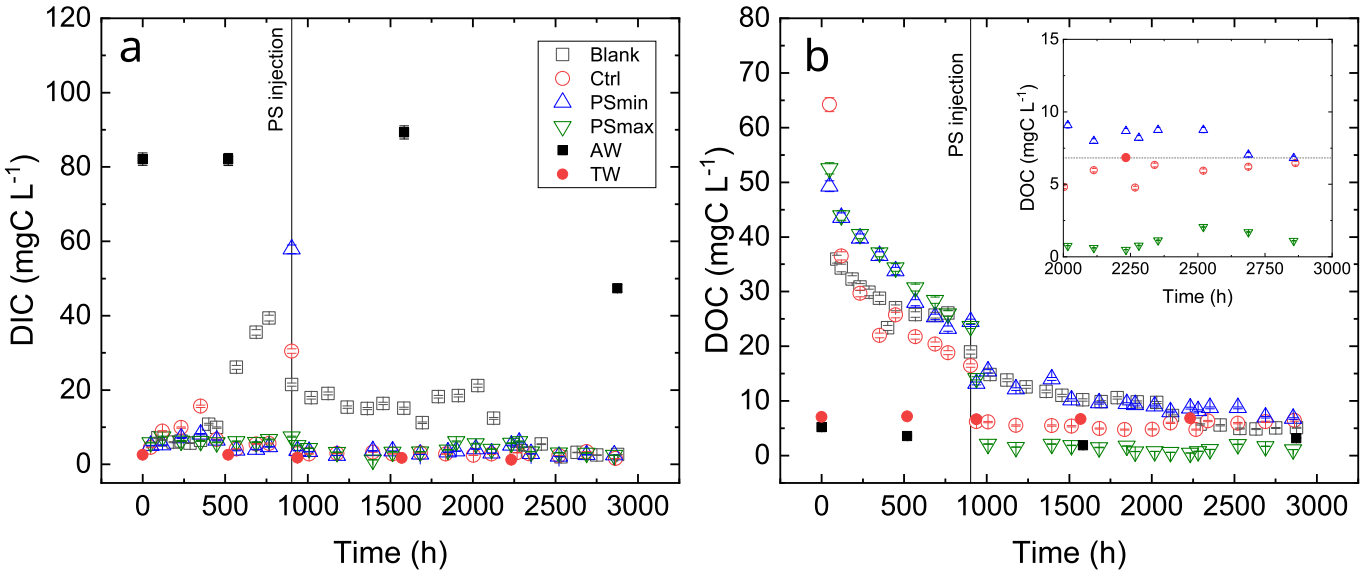

Fig. 6. Dissolved inorganic (DIC) (a) and organic (DOC) (b) carbon of the inlet and outlet solution of each of the flow-through experiments, measured periodically over the experimental time lapse. The lines in each graph indicate the time of the PS injection (for PSmin and PSmax) and the temporary flow rate increase into the columns (except for Blank). Error bars display the analytical uncertainty, and, in some cases, they are smaller than the symbols.

($C_2\overline{S}$), aluminate (C_3A) and aluminoferrite (C_4AF)] together with hydration products [i.e., calcium silicate/aluminate and magnesium hydrates (C-$\overline{S}$ (A,M)-H), and ettringite (AFt) with the typical acicular morphology] (Fig. 11 and "SEM/EDS" section in Supplementary Material).

Notably, after one week of RCG conditioning in TW, dedolomitization processes were already identified on the carbonatic gravel fragments, leading to the formation of a Mg-Al phase (see "SEM/EDS" section in Supplementary Material). Tabular "flake-like" crystals, consistent in chemical composition and morphology with portlandite (CH), were observed on the reacted solid, suggesting that the low amount of initial portlandite (see Fig. 8) did not completely dissolve and/or new portlandite formed after cement re-hydration. The analysis of the concrete after reaction also disclosed massive calcite precipitates, as well as ettringite/thaumasite acicular crystals that piled up into fractures, porosities and outer surface of all the grains (Fig. 12 and "SEM/EDS" section in Supplementary Material). This corroborates the optical microscopy and XRD observations.

3.8. Recycled concrete porosity

The porosity assays (Fig. 13) revealed that the free water absorption capacity slightly increased after the initial RCG (IN) reacted with the AW solution (Blank). To the contrary, a significant decrease of porosity (reflected by lower abs value) was observed after RCG reacted with the TW solution (Ctrl sample), compared to the initial RCG. Afterwards, with PS treatment, there was an increase in porosity, more evident for the PSmax experiment (note that TW solution was allowed to flow in the

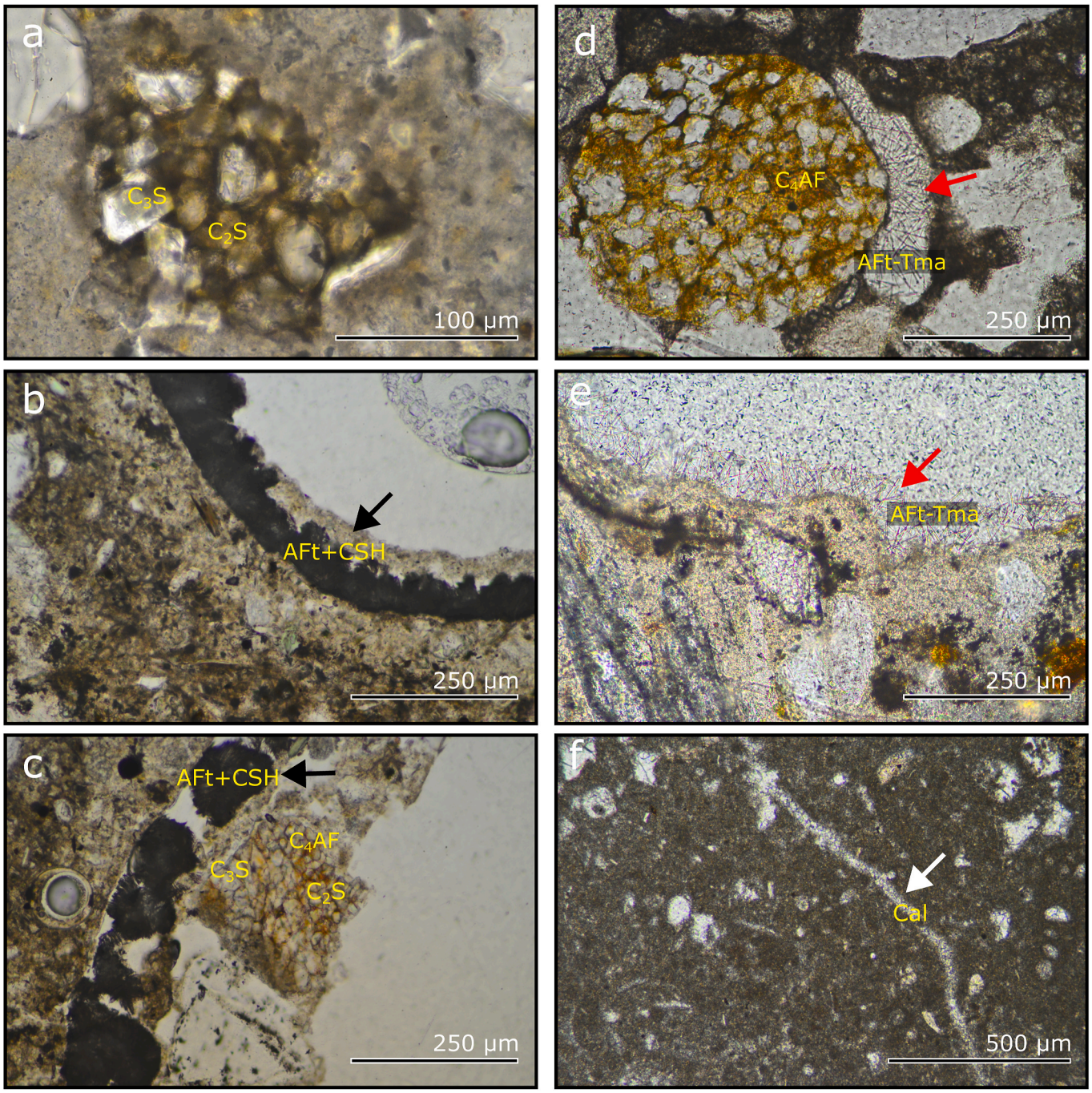

Fig. 7. Photomicrographs of sample thin sections: (a–c) polymictic microconglomerates of the starting material, where anhydrous cement phases ($C_2\overline{S}$, $C_3\overline{S}$) are visible and hydrated products are present as dark areas of acicular crystals (ettringite) between which $C\overline{S}H$ are likely to have formed (black arrows); (d) grain of granitoid lithology retrieved after the Ctrl experiment; (e) polymictic and (f) monomictic microconglomerates retrieved after PSmax experiment. The reacted fragments present some areas where alteration of anhydrous phases is visible. The wall of voids and grains boundaries are covered by acicular crystals (ettringite-thaumasite, AFt-Tma) (red arrows in d and e) and fractures are filled by calcite crystals (withe arrow in f). The brown-colored phase in a, c and d is likely aluminoferrite. (For interpretation of the references to color in this figure legend, the reader is referred to the Web version of this article.)

PS columns before and after the ISCO treatment). Although the differences between free and forced absorption were not statistically significant (values fell within the error), a tendency of the forced absorption to be slightly higher than the free absorption was observed, except for the Blank.

4. Discussion

The production and ubiquitous use of concrete over decades raised concerns about the disposal of residual waste after the dismantling of the infrastructures into which it was incorporated (De Brito and Saikia, 2012; Guo et al., 2018; Ho et al., 2021). The strong alkalinization of solutions circulating through concrete made it a good candidate for a circular economy system where water contaminants may be degraded via i) processes induced by the alkaline conditions or ii) the proposed alkaline-based persulfate ISCO treatment. The results of the flow-through experiments performed in this study highlighted first the effective and durable alkalinization (up to pH 12.1) and buffering

Table 2
Chemical composition (wt. %) of the initial solid material (IN) and the four differently altered RCG samples.

Sample RCG	SiO_2 (%)	Al_2O_3 (%)	Fe_2O_3 (%)	MnO (%)	MgO (%)	CaO (%)	Na_2O (%)	K_2O (%)	TiO_2 (%)	P_2O_5 (%)	SO_3 (%)	LOI (%)	SUM (%)
IN	28.54	5.49	2.35	0.05	2.58	35.19	0.64	1.27	0.26	0.06	0.57	22.80	99.80
Blank	24.66	4.65	1.99	0.04	2.64	39.04	0.54	0.95	0.28	0.06	0.65	24.35	99.85
Control	25.71	5.31	1.94	0.04	2.75	37.24	0.84	1.28	0.24	0.06	0.67	23.71	99.79
PS-min	30.81	5.52	2.42	0.06	2.35	34.61	0.81	1.20	0.28	0.07	0.98	20.63	99.74
PS-max	30.91	6.45	2.89	0.05	2.38	33.47	0.89	1.34	0.29	0.09	1.84	19.20	99.80

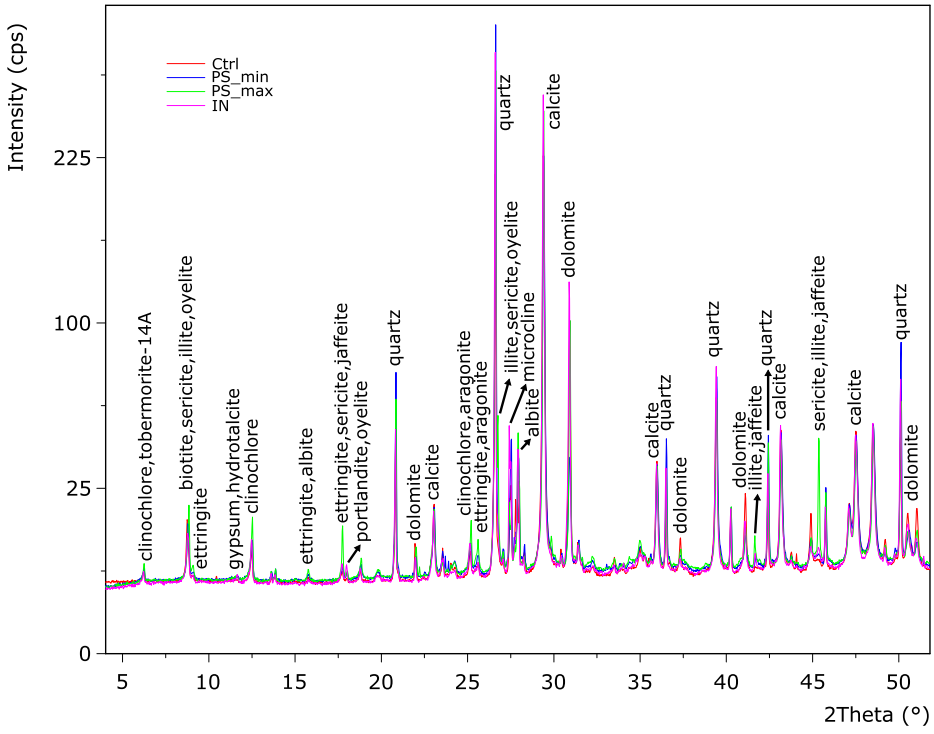

Fig. 8. XRD spectra of the RCG before (IN) and after the flow-through experiments with only TW solution (Ctrl) and with persulfate (PSmin and PSmax).

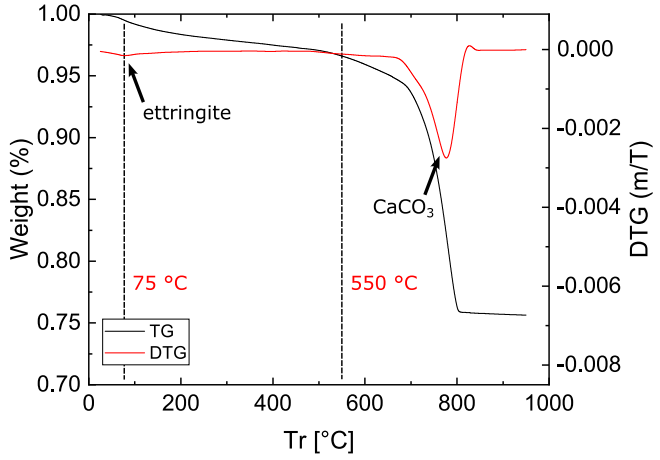

Fig. 9. TG and DTG of a representative sample of the initial RCG.

capacity of the recycled concrete for solutions spanning at initial pH range of 7–11. This robust alkalinization and buffering capacity is crucial for ensuring the activation of persulfate in water ISCO treatments. The results also revealed the complex nature of a multicomponent material, such as concrete, whose interaction with an aqueous solution occurs via a series of processes that take place simultaneously. Dissolution and precipitation of mineral phases, ion exchange or solution and surface complexation (Engelsen et al., 2009, 2017) may proceed during concrete/solution interaction. In this study, the effects of these processes were investigated on both the solid and the solution fractions. To provide a comprehensive understanding of the system evolution, the following sections examine in detail (i) the processes occurring during recycled concrete rehydration prior to persulfate injection, and (ii) the changes induced by PS activation.

4.1. *Effect of recycled concrete rehydration*

As determined by XRD and DTG, the starting material is a mature concrete, in which portlandite has been almost entirely decomposed and gypsum is almost absent, being ettringite the dominant S phase (Figs. 8–10). Both ettringite and portlandite are cement hydration products formed together with C $\overline{S}$ Hs by the following reactions (Saleh and Eskander, 2020; Chu et al., 2021):

$$2C_3\overline{S} + 6H_2O \rightarrow C_3\overline{S}_2 \cdot 3H_2O + 3CH \cdot (Ca(OH)_2, \cdot portlandite) \quad \text{(Eq. 4)}$$

$$2C_2\overline{S} + 4H_2O \rightarrow C_3\overline{S}_2 \cdot 3H_2O + CH \quad \text{(Eq. 5)}$$

$$C_3A + 3CSH_2\ (gypsum) + 26H^+ \rightarrow C_6AS_3H_{32}\ (ettringite) \quad \text{(Eq. 6)}$$

$$C_4AF + 3CSH_2\ (gypsum) + 30H^+ \rightarrow C_6AS_3H_{32} + CH + Fe(OH)_3 \quad \text{(Eq. 7)}$$

In a late stage of the concrete life cycle, when it is exposed to CO_2,

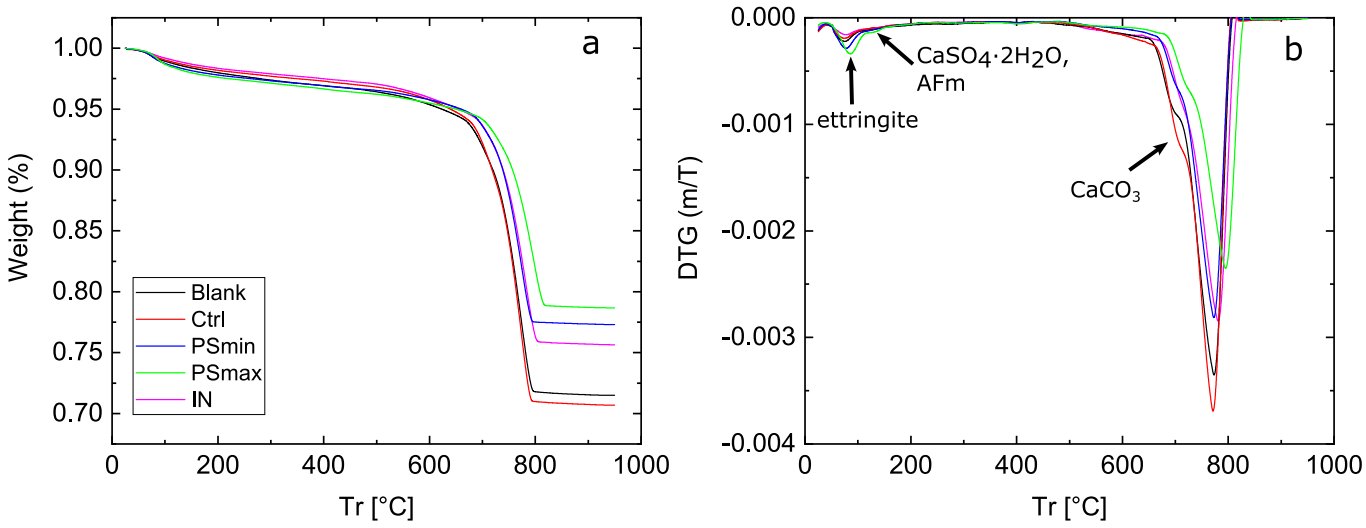

Fig. 10. TG (a) and DTG (b) of a representative sample of the RCG before (IN) and after the flow-through experiments.

Table 3
Relative weight loss of the RCG before (IN) and after the flow-through experiments.

Weight loss %	IN	Blank	Ctrl	PSmin	PSmax
ettringite/AFm	1.03	1.31	1.21	1.54	2.02
organics/CSH	2.35	2.67	2.36	2.23	2.07
$CaCO_3$	20.91	24.48	25.69	18.87	17.19

portlandite may be decomposed by a carbonation process as follows (Steiner et al., 2020; Shen et al., 2022):

$$Ca(OH)_2+CO_2 \rightarrow CaCO_3+H_2O \quad \text{(Eq. 8)}$$

The almost complete dissolution of portlandite triggers the decalcification of C $\overline{S}$ H phases, which plays a fundamental role in the pH buffering at this stage of the concrete maturity (Baston et al., 2012), keeping the active generation of OH^- ions in solution. In the present experiments, the portlandite possibly produced after concrete rehydration, if not carbonated, would immediately dissolve as suggested by the calculated $SI_{Portlandite}$, indicating an undersaturated state in all columns, with values ranging from −3.6 to −1.6.

The complex nature of the material used in this study, with high lithological diversity, gave rise to complex X-ray diffractograms with multiple peaks (Fig. 8). In addition, C $\overline{S}$ H and other amorphous phases (e.g., hydrated aluminate, magnesium and iron phases) that most probably formed during the hydration of the cement phase (Blanc et al., 2010; Bernard et al., 2017; Shen et al., 2022) were likely masked by peaks of other phases and/or were not detected by conventional XRD analysis (Sassi et al., 2024).

During the flow-through alteration experiments, both the concrete aggregates and the cement matrix reacted, contributing to ion enrichment or depletion in the solution and to the formation of secondary mineral phases through dissolution/precipitation processes. Cation and anion concentrations in the solution were therefore controlled by the dissolution of aggregate minerals (i.e., dolomite, calcite, feldspars, phyllosilicates) and anhydrous (i.e., $C_2\overline{S}$, $C_3\overline{S}$, C_3A, C_4AF) and hydrated cement phases, the (re)precipitation of (semi)amorphous (i.e., C $\overline{S}$ H, Al, Mg, Fe hydrates) and crystalline (i., calcite, ettringite, thaumasite, brucite, hydrotalcite, clay minerals) phases, and diagenetic processes (e.g., vermiculite and chlorite formation from micas). The results of chemical analyses in both the solution and solid phases were consistent between each other, showing, in general, that the flow-through systems acted as a sink for some elements (Ca, Mg, S) (Figs. 3 and 5) and a source for others (K, Al) (Figs. 3 and 4).

The proton balance resulted from the solid/solution interaction was quite stable over the experimental time (before persulfate injection), especially for the experiments with TW solution, whose pH maintained at a value of 12.1 with a standard deviation < 0.1. The slightly higher value and lower oscillation of the pH of the TW columns compared with the AW column (12.1 ± 0.1 vs 11.8 ± 0.1, respectively) suggest that, at the flow rate of the experiments, the solution needs more than 2800 h (Blank experiment timelapse) to reach a steady state and that the buffer effect of the system will become more reliable with the time (Fig. 2).

Notably, the Mg concentration was three orders of magnitude richer in AW inlet solution than in TW (Fig. 3b). However, the concentration dropped when the solution started to flow through the column. Similarly, much higher inorganic carbon (DIC, Fig. 6a) was measured in the AW inlet solution. This hints to the precipitation of Mg bearing phases such as Mg-carbonates (hydrotalcite).

Identifying the solubility-controlling phases for each element in a solution/concrete system is not trivial since several reactions may take place according to the thermodynamics of the systems. According with previous studies (Engelsen et al., 2009; Bernard et al., 2017), Mg might be controlled by brucite ($Mg(OH)_2$), which was however not clearly identified by XRD. Nevertheless, $SI_{Brucite}$ (Table S3 in Supplementary Material) ranged from −0.4 to 1.0 (negative SI values were only obtained for the Blank experiment), indicating favorable conditions for its formation. The SEM examination of dolomite ($CaMg(CO_3)_2$) revealed its alteration to hydrotalcite ($Mg_4Al_2(OH)_{12}CO_3{\cdot}2H_2O$) at the rim of the grain during the dedolomitization process (see "SEM/EDS" section in Supplementary Material). $SI_{Dolomite}$ mostly presents negative values, especially early in the experiments, consistent with dolomite dissolution. $SI_{Hydrotalcite}$ values were strongly positive, ranging from 2.8 to 11.3, indicating favorable conditions for its precipitation (Table S3). Therefore, hydrotalcite was probably the phase controlling Mg concentration in the solution, regardless the type of inlet solution used (Blanc et al., 2010; Bernard et al., 2022). Clay minerals (e.g., saponite) may have also contributed to some extent to the balance of total Mg in solution.

The Si, Fe and Al concentration trends, similar in all the conducted experiments (except for Al after PS injection), reflected the leaching of these elements after dissolution of silicates, aluminosilicates and oxides, that tend to a steady state. The explanation of the kinetics of this process has been recently object of intense discussion that includes considerations on dissolution/reprecipitation mechanisms, the formation of amorphous phases and the key role of crystal defects in defining the kinetic pathways (Ruiz-Agudo et al., 2014; Daval et al., 2018; Luttge et al., 2019; Kurganskaya and Luttge, 2021). Despite the complexity of

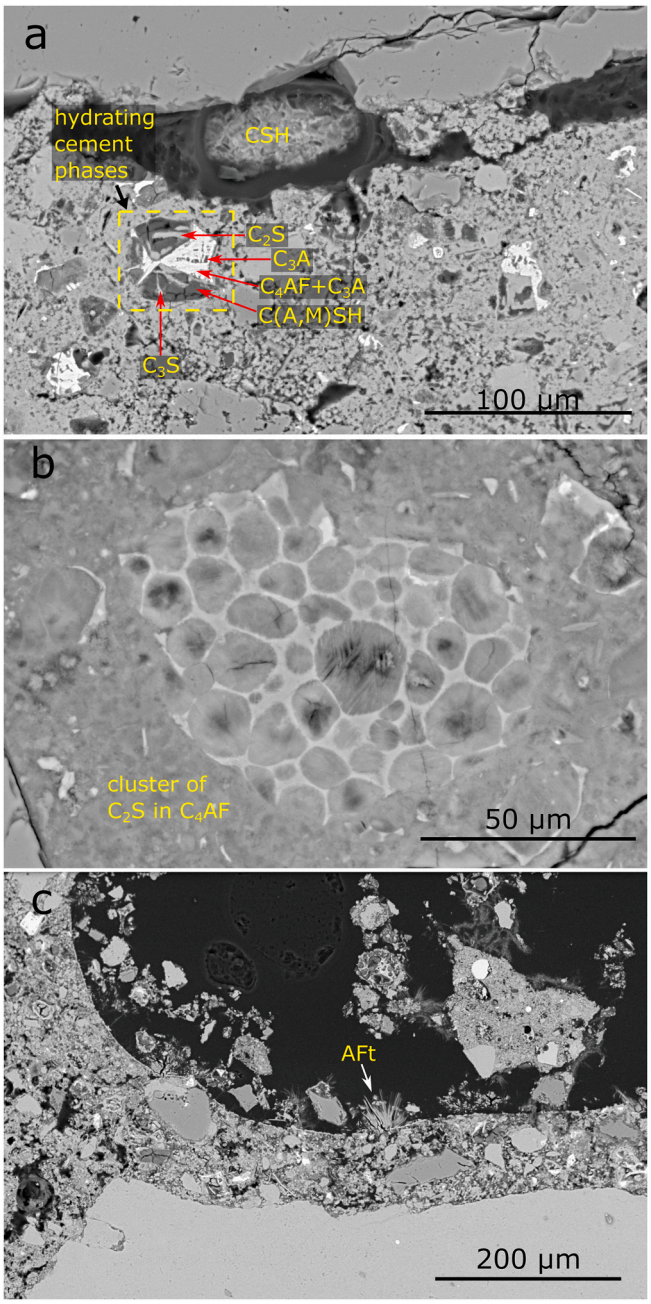

Fig. 11. Back Scattering-SEM images of (a) the RCG and (b,c) the same material after one week of conditioning. Anhydrous phases and hydrated cement products coexist.

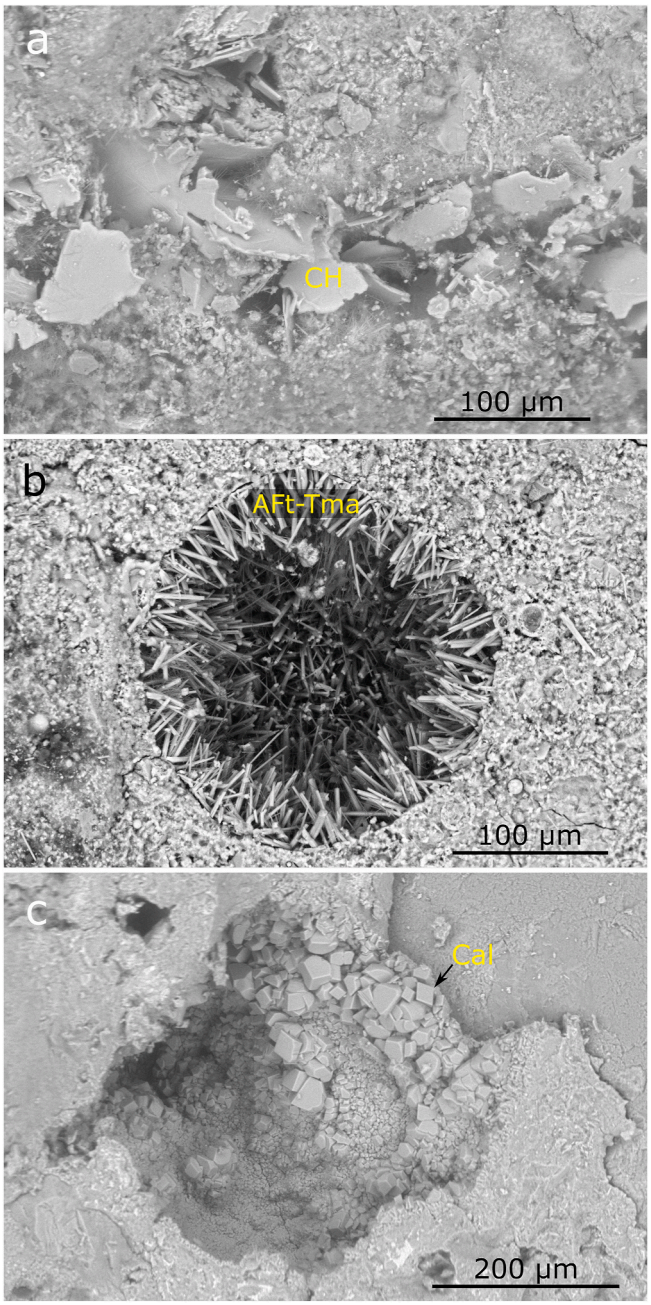

Fig. 12. BS-SEM images of the reacted RCG retrieved from (a) column Ctrl and (b,c) column PSmax at the end of the experiments. The hydration of the cement phases leads to the formation of plate-like crystals of portlandite (CH) (a) and massive precipitation of ettringite/thaumasite acicular crystals (b) especially after PS injection. Precipitation of idiomorphic calcite (Cal) crystals after carbonation of the concrete (c).

the molecular processes associated with the reaction of the different mineral phases composing the concrete, it may be concluded, based on the results of the hydro(geo)chemical calculations (Table S3) and the identified mineral phases (Fig. 8), that:

- The Si concentration was mainly controlled by the dissolution of quartz, since SI_{Quartz} was always negative. However, the formation of C $\overline{S}$ H phases and likely of authigenic clay minerals (Bétard et al., 2009; Engelsen et al., 2009) may contribute to the Si balance in solution ($SI_{CSH} \sim 0$).
- Fe-bearing phases most probably form during cement hydration (Eq. (7)). In the present experiments precipitation was favorable (SI > 0) for ferrihydrite ($Fe(OH)_3$) and goethite (FeOOH). Nevertheless, the poor crystallinity of ferrihydrite hampers its detection by X-ray diffraction when it is in low quantity (Manceau and Drits, 1993), and, in any case, most probably converted to more stable Fe-oxides (e.g., goethite) with time (Carlson and Schwertmann, 1981; Meriot, 2022).
- Al concentration may be controlled by aluminum end-members of CA $\overline{S}$ H phases and ettringite (Blanc et al., 2010; Engelsen et al., 2017). Although Al-hydrated phases (other than ettringite) were not clearly identified in the present study, it can be assumed that the increasing concentration of Al in the outlet solutions depended on the dissolution of those phases and partially of aluminosilicate (biotite, sericite). It is worth noting that the hydrotalcite formation

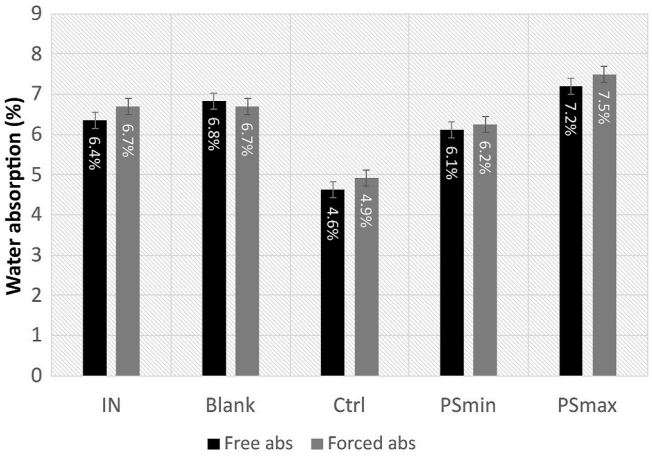

Fig. 13. Porosity estimates of the RCG before (IN) and after the flow-through experiments as free and force absorption values.

as secondary phase would also contribute to the fate of dissolved Al, being however the ettringite the main controlling phase of the total Al in solution.

At the pH range of the experiments, higher than 11 in most cases, calcite was probably the main solubility-controlling phase for Ca (Engelsen et al., 2009). $SI_{Calcite}$ values were positive (ranging from 0.5 to 2.2) regardless of the column conditions, indicating that calcite precipitation would be occurring throughout the whole experiment. In an uncontrolled atmosphere, carbonation of concrete (e.g., Eq. (8)) most certainly occurred. The higher CaO content measured in the reacted solids (without persulfate) (Table 2) compared with the chemical composition of the initial material, supports the precipitation of carbonates, especially from the AW solution (Blank experiment). Moreover C $\overline{S}$ H and CA$\overline{S}$ H phases undoubtedly contributed to the availability of Ca in solution. Ettringite was likely the solubility-controlling phase for S, considering its massive presence in the reacted solid samples and the fact that monosulfate phases (AFm) are not stable at the experimental conditions (Matschei et al., 2007). This is also supported by the near equilibrium conditions (SI ~ 0) of ettringite before the persulfate injection. The formation of ettringite could thus explain the lower concentrations of SO_4^{2-} in the outlet solutions compared to the inlet solutions for the pre-injection period (Fig. 5a) (note that thaumasite would form in very low amount since it is more stable and forms more readily at temperature <15 °C (Glasser et al., 2008)).

4.2. Effect of persulfate injection

The injection of persulfate adds a degree of complexity to the system with the generation of high amounts of protons (which reduces the pH) and sulfate (Eqs. (1)–(3)) and the expected degradation of the organic compounds (here represented by the DOC).

As discussed in the previous section, the RCG maintained its buffering capacity at both tested persulfate dosages, enabling effective persulfate activation. Indeed, the addition of PS resulted in i) a decrease of the pH due to H^+ generation (Fig. 2) and ii) a marked increase in sulfate concentration (Fig. 5a), which led to an oversaturation of sulfate phases such as ettringite (Fig. 12b), with $SI_{Ettringite}$ close to 4 (Table S1). This was especially relevant for the PSmax experiment. Despite the pH drop, the buffer capacity of the solid/solution system promptly re-stabilized the pH to a value near to the material pH (~11.7) thanks to the buffering effect of the C $\overline{S}$ H and CA$\overline{S}$ H phases. This result illustrates the potential of RCG to sustain the high pH conditions required for PS activation in advanced oxidation processes.

Regarding organic matter, although, as indicated in the results section, the initial DOC values measured in the outlet solutions were unexpectedly much higher than those in the inlet solutions (Fig. 6), that was followed by gradual DOC decreasing trends in all columns. This points to the gradual leaching and flush out of the organic compounds that we hypothesized were already present in the system, both in the solid and as residual material from the columns. As all the organic compounds were washed out of the columns between 2000 and 2500 h of experimental time, the outlet DOC matched the inlet value, except for the PSmax experiment, where the concentration dropped almost to zero right after the PS injection (Fig. 6) indicating DOC degradation during PS activation. A PS concentration ten thousand times higher than the DOC (7 mgC L^{-1} vs. 70 gPS L^{-1}, PSmax column) was therefore found to be effective for a rapid degradation. On the other hand, the DOC trend in the PSmin experiment suggests that the minimum persulfate concentration for the degradation of organic compounds in contaminated solution should be more than a thousand times higher than the organics concentration (7 mgC L^{-1} vs. 7 gPS L^{-1}, PSmin column). The significant oxidation of organic matter in the PSmax column was also reflected by the lowest LOI (19.2 wt %, Table 2) and relative weight loss calculated from the TG diagrams (2.07 wt %, Table 3). In this context, it should be noted that the overall reaction path of the persulfate may include radical scavenge interactions with anions (e.g., chloride, carbonate, or bicarbonate) in solution that might decrease the efficiency of the oxidation (Tsitonaki et al., 2010; Petri et al., 2011; Lee et al., 2020). Considering the low concentration of the potential radical scavengers with respect to that of the PS used in this study, the mitigation effect of the oxidant is unlikely and, in any case, neglectable for the PSmax experiment.

It is worth noting that the addition of PS to the solution and its activation apparently fostered the dissolution of calcium species, resulting in an increase on Ca concentration with respect to the inlet solution (Fig. 3). Furthermore, the XRD, XRF and TGA results (Tables 2 and 3; Figs. 6 and 7) showed a decrease in Ca and an increase in S and Al in the solid phase after the injection of the oxidant. The shift of the DTG curve of the PSmax experiment sample towards higher temperatures hints to the formation of more stable calcium carbonate phases (calcite), which would decompose during the temperature rising after more labile phases like C $\overline{S}$ H. This would indicate that the dissolving Ca phases during persulfate addition were mainly C$\overline{S}$ H, corroborated by the higher Ca and Si concentration of the outlet solutions of the PS experiments after injection with respect to the control (Fig. 3a and 4a). In addition, AFm and/or gypsum were detected in the sample as minor phases at the end of the PSmax experiment (peak near to the ettringite phase, Fig. 10). This is in accordance with previous studies (Köhler et al., 2006; Glasser et al., 2008; Zhang et al., 2022), which have shown that sulfate attack on concrete first consumes portlandite, followed by the degradation of C $\overline{S}$ H and leading to the production of gypsum and AFm. On the other hand, the reaction of gypsum with calcium aluminate hydrates and/or Al species in solution produces ettringite (AFt) (Engelsen et al., 2017), whose solubility is much lower than gypsum and AFm phases. Since AFm should be unstable at the experimental conditions (temperature, pH, SO_3/Al_2O_3 and CO_2/Al_2O_3 ratios) re-stabilized after persulfate injection (Matschei et al., 2007; Damidot et al., 2011), the total conversion of AFm to AFt would be expected if the experiment had continued to run. Indeed, SI_{AFm} (mainly monosulfoaluminate, monocarboaluminate and monosulfate-Fe) and SI_{Gypsum} exhibited negative values (SI < 0) in all columns and thus, according to SI calculations, their formation would not be favorable. $SI_{Ettringite}$ evolved from ~0.0 to ~4.0 after persulfate injection, reflecting that the SO_4^{2-} release from persulfate activation (Eqs. (1)–(3)) would trigger ettringite precipitation (a scheme summarizing the main water-solid interactions after PS injection can be found in the graphical abstract and in. Supplementary Material).

The massive formation of ettringite, known for expansion during crystal growth, alongside the increase of the C $\overline{S}$ H decalcification rate, likely provoked the concrete microstructure to fail. This would agree with the higher porosity measured in the solid material after the PSmax

experiment (Fig. 13). To the contrary, when no persulfate was used (Ctrl case), the porosity decreased due to the precipitation of secondary phases (calcite, ettringite) that exerted minimal stress on the structure, although induced a certain degree of clogging as demonstrated by the microporosity increase (forced abs slightly higher than free abs, Fig. 13). Therefore, using RCG in an ISCO treatment via base activation of PS for water decontamination would prevent clogging of the system. At the same time, a more prolonged sulfate attack of the concrete may affect the structural stability of a gravel-filled trench and even decrease the buffering capacity of the material due to degradation of the C $\overline{S}$ H and the possible formation of gel-like materials (Engelsen et al., 2009; Zhang et al., 2022).

Therefore, these results showed that the strong alkalinity conditions provided by the RCG were able to activate the PS, leading to (at a proper DOC/PS ratio) a significant organic matter degradation. This ability of RCG to maintain high pH and activate PS, but also to mitigate clogging risks, supports its use in water remediation projects. Successful field application will require careful consideration of site-specific factors, including the initial composition and maturity of the RCG or groundwater chemistry. Pilot-scale studies are recommended to validate laboratory findings and optimize operational parameters for diverse environmental settings.

5. Conclusions

The analysis of the solid and solution of a laboratory system for ISCO treatment was performed in this study to investigate the potential of RCG in the long-term alkaline activation of the oxidant persulfate and describe the evolution of the material after several months of reaction.

The use of RCG was proven to be effective in maintaining a high pH for the PS activation and in buffering the solution after the oxidant injection. The higher variability and the slightly lower pH value of the outlet solution of the AW experiment suggests that, at the residence time of the performed experiments, a fresh solution would probably need more than 2800 h to reach a steady state and a stable buffer capacity. In contrast, the TW water solution, long equilibrated with concrete material in the interception trench before collection for laboratory experiments, maintained stable pH values over the experiment time, with a good recovering after persulfate injection.

The degradation of the organic compounds in solution was almost complete for a persulfate concentration ten thousand times higher than the organics one. However, useful PS/organic compounds concentration ratios may also fall between the minimum (persulfate a thousand times higher than DOC) and maximum used in the present study.

The complexity of the concrete-solution system required a multi-approach and the use of several techniques that provided complementary information. Based on the observations and analysis performed, in the absence of portlandite the role of C $\overline{S}$ H and aluminum/magnesium hydrates (e.g., CA$\overline{S}$ H) was proven to be crucial for the stability of the concrete microstructure and for maintaining the alkaline pH condition. Together with concrete aggregates and cement phase dissolution, carbonation and (re)precipitation of Ca, Al, Mg and Fe phases were the controlling processes defining the final state of the system.

Finally, two key aspects emerge from the present study:

- By demonstrating the role of recycled concrete in inducing and maintaining alkaline conditions and activating persulfate, and the capacity of the concrete/PS system to mitigate the clogging risks through enhanced porosity, this study underscores its potential use for broader environmental remediation applications. Nevertheless, the duration and number of interventions in a recycled concrete-based ISCO treatment would depend on the initial materials used and the hydrochemistry of the water to be decontaminated. Assessing the maturity (portlandite and C $\overline{S}$ H content) and overall composition (mineral phases) of RCG prior to its use is crucial for predicting the long-term high-pH buffer capacity of the system. Notably, further research is needed to evaluate the system buffering capacity in the long-term, considering the inevitable degradation of the C(A)$\overline{S}$ H during ISCO treatments with PS.
- The findings and comprehensive dataset produced offer a valuable foundation for future assessment of the thermodynamics and kinetics of concrete/solution systems by speciation and transport modelling to unravel the mechanisms driving solid and solution compositional changes. Hence, this study not only will help to understand the applicability of recycled concrete to persulfate-based water decontamination systems but provides fundamental knowledge valuable for the management of similar settings characterized by concrete-fluid interaction.

CRediT authorship contribution statement

Chiara Cappelli: Writing – review & editing, Writing – original draft, Visualization, Supervision, Methodology, Investigation, Formal analysis, Data curation, Conceptualization. **Albert Fernández-Lagunas:** Writing – review & editing, Investigation, Formal analysis, Data curation. **María Usieto:** Investigation, Formal analysis, Data curation. **Mònica Rosell:** Writing – review & editing, Supervision, Methodology, Investigation, Data curation, Conceptualization. **Clara Torrentó:** Writing – review & editing, Supervision, Methodology, Conceptualization. **Cristina Domènech:** Writing – review & editing, Methodology, Conceptualization. **Jordi Palau:** Writing – review & editing, Methodology, Conceptualization. **Albert Soler:** Project administration, Funding acquisition, Conceptualization.

Declaration of generative AI and AI-assisted technologies in the writing process

During the preparation of this work the authors used OpenAI tool (ChatGPT) in order to improve the readability of some sections of the manuscript. After using this tool, the authors reviewed and edited the content as needed and take full responsibility for the content of the published article.

Declaration of competing interest

The authors declare that they have no known competing financial interests or personal relationships that could have appeared to influence the work reported in this paper.

Acknowledgements

This work was financed through REMECLOR project (PDC2021-120861-C21) funded by the Spanish Government (MICIU/AEI/10.13039/501100011033) and by European Union NextGenerationEU/PRTR. Funding was also received from the ADVANCE4WATER-ISOTRACE (PID2022-139911OB-C4-01) project, funded by MICIU/AEI/10.13039/501100011033/FEDER,UE. This work was also supported by the Consolidate Research Group (2021SGR00308), funded by the AGAUR (Agència de Gestió d'Ajuts Universitaris i de Recerca, Government of Catalonia). Chiara Cappelli acknowledges the funding from María Zambrano grant for the attraction of international talent, awarded by the Ministry of Universities of the Government of Spain within the framework of the European Union Next Generation-EU programme. Albert Fernández-Lagunas would also like to thank the AGAUR for the PhD Grant 2022 FI_B 00498 awarded by the Department of Research and Universities of the Government of Catalonia and the co-funding of the European Social Fund Plus (ESF+). We thank all the technicians in MAiMA and Centres Científics i Tecnològics of the Universitat de Barcelona (CCiT-UB) for their support. Chiara Cappelli is also grateful for the support of Prof. M. Esperanza Tauler and Prof. Àngels

Canals of the University of Barcelona.

Appendix A. Supplementary data

Supplementary data to this article can be found online at https://doi.org/10.1016/j.apgeochem.2025.106590.

Data availability

Data will be made available on request.

References

Baston, G.M.N., Clacher, A.P., Heath, T.G., Hunter, F.M.I., Smith, V., Swanton, S.W., 2012. Calcium silicate hydrate (C-S-H) gel dissolution and pH buffering in a cementitious near field. Mineral. Mag. 76, 3045–3053.

Bernard, E., Lothenbach, B., Le Goff, F., Pochard, I., Dauzères, A., 2017. Effect of magnesium on calcium silicate hydrate (C-S-H). Cement Concr. Res. 97, 61–72.

Bernard, E., Zucha, W.J., Lothenbach, B., Mäder, U., 2022. Stability of hydrotalcite (Mg-Al layered double hydroxide) in presence of different anions. Cement Concr. Res. 152, 106674.

Bétard, F., Caner, L., Gunnell, Y., Bourgeon, G., 2009. Illite neoformation in plagioclase during weathering: evidence from semi-arid Northeast Brazil. Geoderma 152, 53–62.

Blanc, Ph, Bourbon, X., Lassin, A., Gaucher, E.C., 2010. Chemical model for cement-based materials: thermodynamic data assessment for phases other than C–S–H. Cement Concr. Res. 40, 1360–1374.

De Brito, J., Kurda, R., 2021. The past and future of sustainable concrete: a critical review and new strategies on cement-based materials. J. Clean. Prod. 281, 123558.

De Brito, J., Saikia, N., 2012. Recycled Aggregate in Concrete: Use of Industrial, Construction and Demolition Waste. Springer Science & Business Media.

Carlson, L., Schwertmann, U., 1981. Natural ferrihydrites in surface deposits from Finland and their association with silica. Geochem. Cosmochim. Acta 45, 421–429.

Chu, D.C., Kleib, J., Amar, M., Benzerzour, M., Abriak, N.-E., 2021. Determination of the degree of hydration of Portland cement using three different approaches: scanning electron microscopy (SEM-BSE) and Thermogravimetric analysis (TGA). Case Stud. Constr. Mater. 15, e00754.

Ciampi, P., Esposito, C., Bartsch, E., Alesi, E.J., Papini, M.P., 2023. Pump-and-treat (P&T) vs groundwater circulation wells (GCW): which approach delivers more sustainable and effective groundwater remediation? Environ. Res. 234, 116538.

Damidot, D., Lothenbach, B., Herfort, D., Glasser, F.P., 2011. Thermodynamics and cement science. Cement Concr. Res. 41, 679–695.

Daval, D., Calvaruso, C., Guyot, F., Turpault, M.-P., 2018. Time-dependent feldspar dissolution rates resulting from surface passivation: experimental evidence and geochemical implications. Earth Planet Sci. Lett. 498, 226–236.

Deloye, F.X., Divet, L., 1992. The alkali-aggregate reaction - quantitative aspects. In A. B. Poole (Ed.), Proceedings of the 9th International Conference on Alkali-Aggregate Reaction in Concrete (Concrete Society Publication CS.104), Volume 1, London, pp. 251–260.

Engelsen, C.J., van der Sloot, H.A., Petkovic, G., 2017. Long-term leaching from recycled concrete aggregates applied as sub-base material in road construction. Sci. Total Environ. 587–588, 94–101.

Engelsen, C.J., van der Sloot, H.A., Wibetoe, G., Petkovic, G., Stoltenberg-Hansson, E., Lund, W., 2009. Release of major elements from recycled concrete aggregates and geochemical modelling. Cement Concr. Res. 39, 446–459.

Furman, O.S., Teel, A.L., Watts, R.J., 2010. Mechanism of base activation of persulfate. Environ. Sci. Technol. 44, 6423–6428.

Giffaut, E., Grivé, M., Blanc, Ph, Vieillard, Ph, Colàs, E., Gailhanou, H., Gaboreau, S., Marty, N., Madé, B., Duro, L., 2014. Andra thermodynamic database for performance assessment: thermochimie. Appl. Geochem. 49, 225–236.

Glasser, F.P., Marchand, J., Samson, E., 2008. Durability of concrete — degradation phenomena involving detrimental chemical reactions. Cement Concr. Res. 38, 226–246.

Gomes, H.I., Mayes, W.M., Rogerson, M., Stewart, D.I., Burke, I.T., 2016. Alkaline residues and the environment: a review of impacts, management practices and opportunities. J. Clean. Prod. 112, 3571–3582.

Guo, H., Shi, C., Guan, X., Zhu, J., Ding, Y., Ling, T.-C., Zhang, H., Wang, Y., 2018. Durability of recycled aggregate concrete – a review. Cem. Concr. Compos. 89, 251–259.

Ho, H.-J., Iizuka, A., Shibata, E., 2021. Chemical recycling and use of various types of concrete waste: a review. J. Clean. Prod. 284, 124785.

Institution, B.S., 2008. Natural Stone Test Methods: Determination of Water Absorption at Atmospheric Pressure. British Standards Institution.

Kisku, N., Joshi, H., Ansari, M., Panda, S.K., Nayak, S., Dutta, S.C., 2017. A critical review and assessment for usage of recycled aggregate as sustainable construction material. Constr. Build. Mater. 131, 721–740.

Köhler, S., Heinz, D., Urbonas, L., 2006. Effect of ettringite on thaumasite formation. Cement Concr. Res. 36, 697–706.

Krembs, F.J., Siegrist, R.L., Crimi, M.L., Furrer, R.F., Petri, B.G., 2010. ISCO for groundwater remediation: analysis of field applications and performance. Groundwater Monitor. Remed. 30, 42–53.

Kurganskaya, I., Luttge, A., 2021. Mineral dissolution kinetics: pathways to equilibrium. ACS Earth Space Chem. 5, 1657–1673.

Lee, J., von Gunten, U., Kim, J.-H., 2020. Persulfate-based advanced oxidation: critical assessment of opportunities and roadblocks. Environ. Sci. Technol. 54, 3064–3081.

Luttge, A., Arvidson, R.S., Fischer, C., Kurganskaya, I., 2019. Kinetic concepts for quantitative prediction of fluid-solid interactions. Chem. Geol. 504, 216–235.

Ma, F., Zhang, Q., Wu, B., Peng, C., Li, N., Li, F., Gu, Q., 2018. Treatment of PAH-contaminated soil using cement-activated persulfate. Environ. Sci. Pollut. Control Ser. 25, 887–895.

Manceau, A., Drits, V.A., 1993. Local structure of ferrihydrite and Feroxyhite by Exafs Spectroscopy. Clay Miner. 28, 165–184.

Matschei, T., Lothenbach, B., Glasser, F.P., 2007. The AFm phase in Portland cement. Cement Concr. Res. 37, 118–130.

Meriot, A., 2022. Structure and Reactivity of Industrial Calcium Ferrites (Brownmillerite) and their Hydrates Concerning Aqueous Sulfated Solutions.

Naik, T.R., 2008. Sustainability of concrete construction. Pract. Period. Struct. Des. Construct. 13, 98–103.

O'Connor, D., Hou, D., Ok, Y.S., Song, Y., Sarmah, A.K., Li, X., Tack, F.M.G., 2018. Sustainable in situ remediation of recalcitrant organic pollutants in groundwater with controlled release materials: a review. J. Contr. Release 283, 200–213.

Palau, J., Marchesi, M., Chambon, J.C.C., Aravena, R., Canals, À., Binning, P.J., Bjerg, P. L., Otero, N., Soler, A., 2014. Multi-isotope (carbon and chlorine) analysis for fingerprinting and site characterization at a fractured bedrock aquifer contaminated by chlorinated ethenes. Sci. Total Environ. 475, 61–70.

Parkhurst, D.L., Appelo, C.A.J., Survey, U.S.G., 2013. Description of input and examples for PHREEQC version 3: a computer program for speciation, batch-reaction. One-Dimensional Transport, and Inverse Geochemical Calculations. Reston, vol. A.

Petri, B.G., Watts, R.J., Tsitonaki, A., Crimi, M., Thomson, N.R., Teel, A.L., 2011. Fundamentals of ISCO using persulfate. In: Siegrist, R.L., Crimi, M., Simpkin, T.J. (Eds.), In Situ Chemical Oxidation for Groundwater Remediation. Springer, New York, New York, NY, pp. 147–191.

Rodríguez-Fernández, D., Torrentó, C., Palau, J., Marchesi, M., Soler, A., Hunkeler, D., Domènech, C., Rosell, M., 2018. Unravelling long-term source removal effects and chlorinated methanes natural attenuation processes by C and Cl stable isotopic patterns at a complex field site. Sci. Total Environ. 645, 286–296.

Ruiz-Agudo, E., Putnis, C.V., Putnis, A., 2014. Coupled dissolution and precipitation at mineral–fluid interfaces. Chem. Geol. 383, 132–146.

Russell, K.T., Rabideau, A.J., 2000. Decision analysis for Pump-and-Treat design. Groundwater Monitor. Remed. 20, 159–168.

Saleh, H.M., Eskander, S.B., 2020. 18 - innovative cement-based materials for environmental protection and restoration. In: Samui, P., Kim, D., Iyer, N.R., Chaudhary, S. (Eds.), New Mater. Civil Eng. 613–641. Butterworth-Heinemann.

dos Santos Macedo, R., Ulsen, C., Mueller, A., 2019. Quantification of residual cement paste on recycled concrete aggregates containing limestone by selective dissolution. Constr. Build. Mater. 229, 116875.

Sassi, M., Qafoku, O., Bowden, M.E., Pearce, C.I., Latta, D., Miller, Q.R.S., Boamah, M.D., N'Diaye, A.T., Holliman, Jr.J.E., Arenholz, E., Rosso, K.M., 2024. Influence of time and ageing conditions on the properties of ferrihydrite. Environ. Sci. Nano 11, 1682–1692.

Shen, P., Zhang, Y., Jiang, Y., Zhan, B., Lu, J., Zhang, S., Xuan, D., Poon, C.S., 2022. Phase assemblance evolution during wet carbonation of recycled concrete fines. Cement Concr. Res. 154, 106733.

Snellings, R., Chwast, J., Cizer, Ö., De Belie, N., Dhandapani, Y., Durdzinski, P., Elsen, J., Haufe, J., Hooton, D., Patapy, C., Santhanam, M., Scrivener, K., Snoeck, D., Steger, L., Tongbo, S., Vollpracht, A., Winnefeld, F., Lothenbach, B., 2018. RILEM TC-238 SCM recommendation on hydration stoppage by solvent exchange for the study of hydrate assemblages. Mater. Struct. 51, 172.

Srivastava, V.J., Hudson, J.M., Cassidy, D.P., 2016. In situ solidification and in situ chemical oxidation combined in a single application to reduce contaminant mass and leachability in soil. J. Environ. Chem. Eng. 4, 2857–2864.

Steiner, S., Lothenbach, B., Proske, T., Borgschulte, A., Winnefeld, F., 2020. Effect of relative humidity on the carbonation rate of portlandite, calcium silicate hydrates and ettringite. Cement Concr. Res. 135, 106116.

Thomas, J., Thaickavil, N.N., Wilson, P.M., 2018. Strength and durability of concrete containing recycled concrete aggregates. J. Build. Eng. 19, 349–365.

Torrentó, C., Audí-Miró, C., Bordeleau, G., Marchesi, M., Rosell, M., Otero, N., Soler, A., 2014. The use of alkaline hydrolysis as a novel strategy for chloroform remediation: the feasibility of using construction wastes and evaluation of carbon isotopic fractionation. Environ. Sci. Technol. 48, 1869–1877.

Tsitonaki, A., Petri, B., Crimi, M., Mosbk, H., Siegrist, R.L., Bjerg, P.L., 2010. In situ chemical oxidation of contaminated soil and groundwater using persulfate: a review. Crit. Rev. Environ. Sci. Technol. 40, 55–91.

Verian, K.P., Ashraf, W., Cao, Y., 2018. Properties of recycled concrete aggregate and their influence in new concrete production. Resour. Conserv. Recycl. 133, 30–49.

Villain, G., Thiery, M., Platret, G., 2007. Measurement methods of carbonation profiles in concrete: thermogravimetry, chemical analysis and gammadensimetry. Cement Concr. Res. 37, 1182–1192.

Wang, C., Chazallon, C., Braymand, S., Hornych, P., 2024. Thermogravimetric analysis (TGA) for characterization of self-cementation of recycled concrete aggregates in pavement. Thermochim. Acta 733, 179680.

Wang, R., Yu, N., Li, Y., 2020. Methods for improving the microstructure of recycled concrete aggregate: a review. Constr. Build. Mater. 242, 118164.

Xie, T., Dang, Z., Zhang, J., Zhang, Q., Zhang, R.-H., Liao, C.-J., Lu, G.-N., 2021. Decontamination of dense nonaqueous-phase liquids in groundwater using pump-

and-treat and in situ chemical oxidation processes: a field test. RSC Adv. 11, 4237–4246.
Zhang, Z., Geng, O., Ma, Z., Ji, Y., Xu, Z., Gao, F., Zhang, J., 2022. Study on the deterioration mechanism of alkali dissolution of concrete mixed with Na2SO4 in external water sources. Constr. Build. Mater. 356, 129283.
Zhang, Z., Scherer, G.W., 2021. Physical and chemical effects of isopropanol exchange in cement-based materials. Cement Concr. Res. 145, 106461.